

Sulfated hyaluronic acid inhibits the hyaluronidase CEMIP and regulates the HA metabolism, proliferation and differentiation of fibroblasts

Anja Schmaus^{a,b}, Melanie Rothley^{a,b}, Caroline Schreiber^a, Stephanie Möller^c, Sven Roßwag^a, Sandra Franz^d, Boyan K. Garvalov^a, Wilko Thiele^{a,b}, Sofia Spataro^e, Carsten Herskind^f, Marco Prunotto^e, Ulf Anderegg^d, Matthias Schnabelrauch^c and Jonathan Sleeman^{a,b}

a - European Center for Angioscience (ECAS), Medical Faculty Mannheim, Heidelberg University, Ludolf-Krehl-Str. 13-17 68167, Mannheim 68167, Germany

b - Institute for Biological and Chemical Systems - Biological Information Processing (IBCS - BIP), Karlsruhe Institute for Technology (KIT), 3640, Postfach Karlsruhe 76021, Germany

c - Biomaterials Department, INNOVENT e.V., Prussingstrasse 27b, Jena 07745, Germany

d - Department of Dermatology, Venerology and Allergology, Faculty of Medicine, Leipzig University, Johannisallee 30, Leipzig 04103, Germany

e - Institute of Pharmaceutical Sciences of Western Switzerland, University of Geneva, Rue Michel-Servet 1, 1211 Geneva 4, Switzerland

f - Department of Radiation Oncology, Universitätsmedizin Mannheim, Medical Faculty Mannheim, Heidelberg University, Theodor-Kutzer-Ufer 1-3, Mannheim 68167, Germany

Corresponding to Anja Schmaus: European Center for Angioscience (ECAS), Medical Faculty Mannheim, Heidelberg University, Ludolf-Krehl-Str. 13 17, 68167 Mannheim, Germany. anja.schmaus@medma.uni-heidelberg.de.

Abstract

Hyaluronan (HA) is an extracellular matrix component that regulates a variety of physiological and pathological processes. The function of HA depends both on its overall amount and on its size, properties that are controlled by HA synthesizing and degrading enzymes. The lack of inhibitors that can specifically block individual HA degrading enzymes has hampered attempts to understand the contribution of individual hyaluronidases to different physiological and pathological processes. CEMIP is a recently discovered hyaluronidase that cleaves HA through mechanisms and under conditions that are distinct from those of other hyaluronidases such as HYAL1 or HYAL2. The role of its hyaluronidase activity in physiology and disease is poorly understood. Here, we characterized a series of sulfated HA derivatives (sHA) with different sizes and degrees of sulfation for their ability to inhibit specific hyaluronidases. We found that highly sulfated sHA derivatives potently inhibited CEMIP hyaluronidase activity. One of these compounds, designated here as sHA3.7, was characterized further and shown to inhibit CEMIP with considerable selectivity over other hyaluronidases. Inhibition of CEMIP with sHA3.7 in fibroblasts, which are the main producers of HA in the interstitial matrix, increased the cellular levels of total and high molecular weight HA, while decreasing the fraction of low molecular weight HA fragments. Genetic deletion of CEMIP in mouse embryonic fibroblasts (MEFs) produced analogous results and confirmed that the effects of sHA3.7 on HA levels were mediated by CEMIP inhibition. Importantly, both CEMIP deletion and its inhibition by sHA3.7 suppressed fibroblast proliferation, while promoting differentiation into myofibroblasts, as reflected in a lack of CEMIP in myofibroblasts within skin wounds in experimental mice. By contrast, adipogenic and osteogenic differentiation were attenuated upon CEMIP loss or inhibition. Our results demonstrate the importance of CEMIP for the HA metabolism, proliferation and differentiation of fibroblasts, and suggest that inhibition of CEMIP with sulfated HA derivatives such as sHA3.7 has potential utility in pathological conditions that are dependent on CEMIP function.

Introduction

The extracellular matrix (ECM) constituent hyaluronic acid (HA) is a glycosaminoglycan comprised of up to 25,000 tandem repeats of glucuronic acid and N-acetylglucosamine. Fibroblasts are the main producers of HA in the interstitial matrix. Recent evidence suggests that HA regulates fibroblast proliferation and motility, and fibroblast-to-myofibroblast differentiation [1]. Accordingly, fibroblasts and HA play a key role in many physiological and pathological conditions, such as wound healing, inflammation, tumor progression and fibrotic processes [1,2]. Importantly, the biochemical properties and cellular roles of HA depend not only on its total levels but also on its molecular size. These are tightly regulated by its synthesis through HA synthases (HAS) and by degradation through hyaluronidases and other mechanisms.

In healthy tissues, HA is mainly present as a high molecular weight (HMW) polymer, and contributes to the formation of the ECM and to tissue homeostasis. HA metabolism is perturbed upon tissue injury, in various inflammatory and fibrotic diseases, and in malignancies [2,3]. In these contexts, increased HA synthesis in conjunction with increased breakdown can lead to the accumulation of HA of different sizes within the extracellular milieu. Low molecular weight HA (LMW-HA) and especially small HA oligosaccharides of 10 kDa or less exert a number of biological effects not observed with HMW-HA, including the induction of inflammatory responses, the activation of dendritic cells and the stimulation of angiogenesis and lymphangiogenesis [3]. Intermediate-sized HA fragments also appear to have specific functions [4], although their biological effects remain to be fully investigated.

In mammals, different hyaluronidases enzymatically cleave HA through hydrolysis of the β -1,4 glycosidic bond. The major mechanism of HA turnover in somatic tissues has been considered until recently to involve initial cleavage of HA by the hyaluronidase HYAL2 at the cell membrane, followed by further degradation by HYAL1, which is present in the extracellular space and in lysosomes [5,6]. This paradigm has become more complicated in recent years with the discovery that the secreted protein CEMIP (Cell migration-inducing and hyaluronan-binding protein, also called KIAA1199 or Hybid) possesses hyaluronidase activity. CEMIP-mediated HA binding and hydrolysis differs mechanistically from other hyaluronidases. Its HA degradation requires the presence of cells, and seems to involve re-internalization of the enzyme together with HA via the clathrin-coated pit pathway [7–9]. CEMIP binds to and degrades HA of different sizes, and can produce HA fragments of less than 10 kDa in size, similar to HYAL1 [7,8,10]. The relative contribution of CEMIP

and other hyaluronidases to physiological and pathological processes remains to be investigated.

CEMIP expression has been linked to a number of fibrotic and malignant diseases, although the role of its hyaluronidase activity in these contexts remains to be demonstrated. For example, CEMIP has been implicated in regulating HA metabolism in fibroblasts [11–13]. Given the importance of HA for fibroblast function, the hyaluronidase activity of CEMIP might play an important role in these cells. High CEMIP expression in skin fibroblasts correlates with skin wrinkling and sagging in photoaged skin [14,15]. Furthermore, CEMIP is involved in endochondral ossification and is also expressed in fibroblasts and chondrocytes of osteoarthritis and rheumatoid arthritis patients. In these cells, CEMIP regulates HA levels and sizes and also induces a fibrosis-like process, features which are thought to be important for disease progression [11,16–19]. For a number of cancers, including breast cancer, gastric cancer and pancreatic ductal carcinoma, expression of CEMIP correlates with poor prognosis [20–23]. CEMIP can promote proliferation, migration and invasion of tumor cells and increase metastasis formation in experimental animals [20–25]. CEMIP-containing exosomes secreted from tumor cells have recently been shown to modify the brain vascular niche and thereby foster brain metastasis [26]. Again, it remains unclear whether the tumor-promoting activity of CEMIP is dependent on its HA degrading activity, in part due to a lack of inhibitors for the CEMIP hyaluronidase activity.

Given the role of hyaluronidases in different diseases, there have been attempts to develop hyaluronidase inhibitors for therapeutic purposes. Examples include L-ascorbic acid 6-hexadecanoate [27,28], dextran sulfate [29], sulfated hyaluronic acid [30–32], flavinoid derivatives [33], the antibiotic hyalurolysin [34] and glycyrrhizin [30,35]. Of these, sulfated hyaluronic acid (sHA) has received the most attention. It is able to inhibit HYAL1 most potently, but also reduces bee venom hyaluronidase and testicular hyaluronidase activity [30], and exerts biological activity in prostate and bladder cancer models [31,32]. The ability of sHA to inhibit the hyaluronidase activity of CEMIP has not been assessed.

In this study, we found that highly sulfated HA derivatives profoundly inhibit CEMIP hyaluronidase activity. Compared to HYAL1, sHA inhibits CEMIP hyaluronidase activity 22-fold more potently. Treatment of fibroblasts with sHA phenocopied genetic loss of CEMIP in fibroblasts at a number of levels, including pericellular accumulation of HMW-HA, reduced proliferation, increased myofibroblast differentiation, and reduced osteogenic and adipogenic differentiation. Together, our data suggest that inhibition of CEMIP with sulfated HA derivatives could be useful therapeutically for a number of pathological conditions.

Results

Sulfated HA derivatives potently inhibit CEMIP hyaluronidase activity

To compare the ability of sulfated HA derivatives to inhibit the hyaluronidase activity of CEMIP and HYAL1, we first established hyaluronidase activity assays for HYAL1 and CEMIP using transient transfections in 293T cells. As shown by agarose gel electrophoresis, both enzymes degrade HA (Supplementary Figure 1). As previously reported [9], we found that degradation of HA by secreted CEMIP takes place under physiological conditions at neutral pH, and requires the presence of cells for hyaluronidase activity to be evident (Supplementary Figure 1). On the other hand, secreted HYAL1 is only active under acidic conditions [36] and exhibits hyaluronidase activity in the absence of cells (Supplementary Figure 1).

Next we analyzed the potency of two differentially sulfated HA derivatives to inhibit the hyaluronidase activity of HYAL1 and CEMIP. In the following experiments, we used a low-sulfated HA (sHA1.2, DS = 1.2) and a highly sulfated HA (sHA3.7, DS = 3.7), respectively. The respective degree of substitution (DS) of the polymers refers to the average number of sulfate groups per repeating disaccharide unit of the HA. Interestingly, sHA3.7 had a much stronger inhibitory effect on HYAL1 and CEMIP compared to sHA1.2, and was able to completely inhibit HA degradation at low concentrations (Fig. 1A and B). In contrast, sHA1.2 and sHA3.7 only weakly inhibited bovine testicular hyaluronidase (BTH) at these concentrations, indicative of different inhibitory mechanisms (Fig. 1C). Delcore (hyaluronan modified with oleic acid) was used as a further control, and did not exhibit any inhibitory effect on the hyaluronidases tested. Titration experiments revealed that sHA3.7 inhibits mouse CEMIP with an IC_{50} of 9.6 nM and HYAL1 with an IC_{50} of 210 nM under the experimental conditions used (Fig. 1D, E, F and G) representing a 22-fold higher potency for CEMIP inhibition compared to HYAL1 inhibition. Additional hyaluronidase assays with cells expressing human CEMIP showed that sHA3.7 inhibits human CEMIP with a similar efficiency (Fig. 1H).

To assess in more detail how the number and position of sulfate groups and the size of the molecules affects their ability to inhibit CEMIP we evaluated HA derivatives with different characteristics (Supplementary Fig. 2A). The results showed that the degree of sulfation is proportional to the ability of HA derivatives to inhibit CEMIP activity. The most highly sulfated HA showed the highest potency, but interestingly, sHA with an average sulfation degree of 2 already showed substantial inhibition of CEMIP

activity (Supplementary Fig. 2B). Furthermore, our results suggest that the size of the sHA molecules is also important. Although highly sulfated HA (DS 3.4 - 3.7) of different molecular weight (20 - 110 kDa) inhibits CEMIP to similar levels, sulfated HA of less than 10 kDa (sHA2.5) shows a clearly reduced potency to inhibit CEMIP (Supplementary Fig. 2B). This is reminiscent of other molecular size-dependent functions of hyaluronan [37], and might suggest that a minimum size of sulfated HA of around 10 kDa is required for CEMIP inhibition.

In further experiments we assessed the influence of chondroitin-6-sulfate and chondroitin-4-sulfate, two closely related glycosaminoglycans that carry a single sulfate group per constituent disaccharide, on CEMIP hyaluronidase activity. Although both chondroitin sulfates inhibited bovine testicular hyaluronidase (data not shown and [38]), neither chondroitin-4-sulfate nor chondroitin-6-sulfate had an influence on the hyaluronidase activity of CEMIP (Supplementary Fig. 3). This suggests that one sulfate group per disaccharide in a glycosaminoglycan is not sufficient to inhibit CEMIP, and/or that the specific structural differences between hyaluronan and chondroitin (which contain N-acetylglucosamine and N-acetylgalactosamine subunits, respectively) is also important. Together, these data show that sulfated HA, especially HA derivatives with a sulfation degree of at least two, are potent inhibitors of the CEMIP hyaluronidase activity, in contrast to endogenously occurring chondroitin sulfates.

Loss of CEMIP or its inhibition with sHA3.7 suppress the degradation of cellular HA

To investigate the cellular functions of CEMIP and the impact of HA with low and high sulfation levels on endogenous HA metabolism, we used fibroblasts that are known to produce high amounts of HA and also express CEMIP ([11,39], Fig. 3A). Treatment of cultured mouse embryonic fibroblasts (MEFs) with sHA3.7 but not with sHA1.2 or Delcore, led to increased levels of pericellular HA, as evidenced by fluorescent staining of HA (Fig. 2A and B). We also purified cell-associated HA from MEFs (cellular HA) and from their conditioned media (free HA) and found that sHA3.7 inhibited release of HA into the culture medium and led to a complete loss of HA degradation products (Fig. 2C). These data demonstrate that highly sulfated HA significantly influences HA metabolism in fibroblasts.

To verify that sHA3.7 modifies HA metabolism through inhibiting CEMIP, we used MEFs from transgenic CEMIP^{fllox/fllox} mice [40] and inactivated CEMIP through adenovirally-driven Cre expression. The impact of genetic deletion of CEMIP on HA metabolism was then assessed. Efficient and stable loss of CEMIP protein in the cells after transduction was confirmed by Western Blot analysis (Fig. 3A).

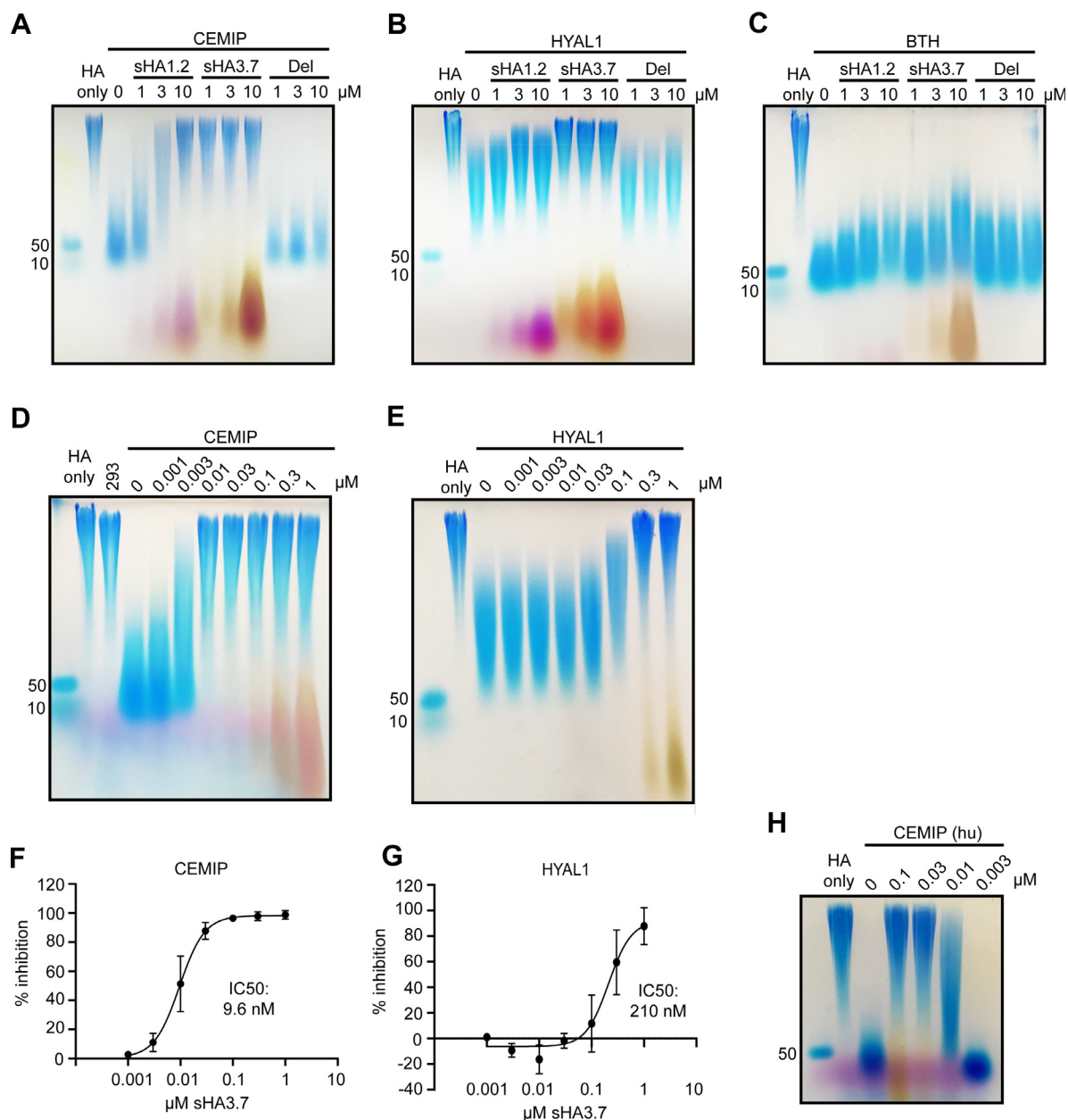


Fig. 1. Highly sulfated HA is a much more potent inhibitor of CEMIP than of HYAL1 or BTH. HA was analyzed by agarose gel electrophoresis and stained with Stains-All. Note that sHA1.2 and sHA3.7 are visible on the lower part of the gel. The substances migrate faster in the gel compared to hyaluronan due to their sulfation. Each experiment was repeated at least 3 times. Representative results are shown. **(A, D)** Hyaluronidase activity of murine CEMIP was analyzed in transiently transfected 293T cells, which were cultivated for 72 hours with HA and with or without the indicated concentrations of sHA1.2, sHA3.7 or Delcore (Del) (A) or sHA3.7 (D). **(B, E)** For HYAL1 activity assays, conditioned media of 293T cells transiently transfected with HYAL1 expression plasmids was mixed with HA and with or without the indicated concentrations of sHA1.2, sHA3.7 or Delcore (Del) (B) or sHA3.7 (E). **(C)** 0.1 U/ml BTH was incubated with HA and 1, 3 or 10 μM sHA1.2, sHA3.7 or Delcore (Del). **(F, G)** Quantification of CEMIP and HYAL1 activity assays, as described in Materials and Methods. Data represent the mean ± SE (n=3). **(H)** Hyaluronidase activity of human CEMIP was analyzed in stably transfected 293T cells which were cultivated with HA and with or without the indicated concentrations of sHA3.7. **(A-H)** As controls, HA was incubated in buffer or in medium without cells (HA only) or with untransfected 293T cells (293), without enzymes.

Interestingly, the absence of CEMIP in MEFs led to similar changes in HA metabolism as sHA3.7 treatment. In both CEMIP KO and sHA3.7 treated cells,

we observed a significant increase in cellular HA levels compared to wild type controls (Fig. 3B and C). Furthermore, we observed a pronounced decrease

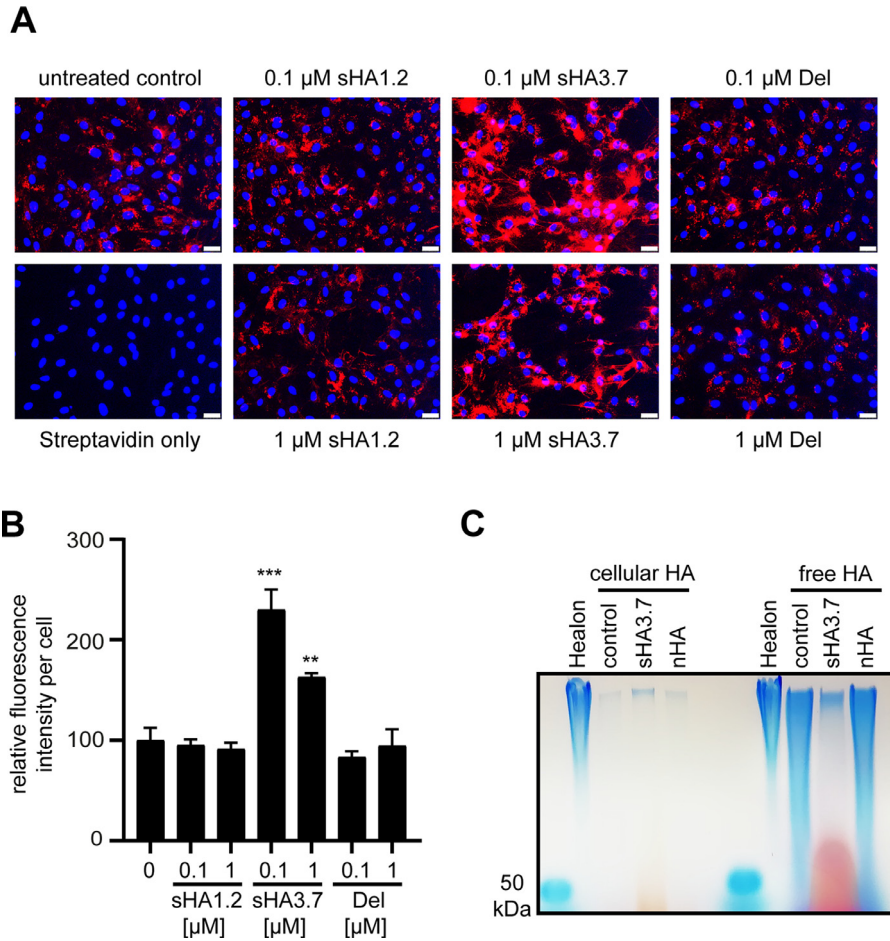


Fig. 2. Sulfated HA influences the HA metabolism of fibroblasts. **(A, B)** sHA3.7 increases the amount of pericellular HA. MEFs were cultivated with DMEM, 10% FCS in chamber slides and were left untreated or treated for 72 hours with 0.1 or 1 μ M sHA1.2, sHA3.7 or Delcore (Del). HA was detected with a biotinylated HA binding protein (HABP) and fluorescently labelled streptavidin. **(A)** Representative images. Scale bar 50 μ m. **(B)** HABP staining intensity was quantified in 6 images per condition. Data represent the mean \pm SE (n=6). Significant differences between untreated and treated samples are indicated. **p < 0.005; ***p < 0.001 (One-way ANOVA). **(C)** sHA3.7 treatment decreases the amount of HA in the conditioned medium of fibroblasts. MEFs were cultivated for 4 days with 1 μ M sHA3.7, nHA (unmodified HA fragments of similar size) or were left untreated. HA was subsequently purified from the cells and the conditioned media, then analyzed by agarose gel electrophoresis and stained with Stains-All. Healon (5 MDa) and 50 kDa HA fragments were used as size standards. The dark spot at the bottom of the gel corresponds to sHA3.7 which is purified together with HA and migrates faster due to its higher negative charge. For all experiments, results were reproduced at least three times, using independent MEF lines. One representative example is shown.

in degraded HA in the conditioned media of both CEMIP KO and sHA3.7 treated cells compared to the respective controls (Fig. 3D and E). Together, these results suggest that sHA3.7 regulates HA metabolism in MEFs mainly via inhibition of CEMIP, and that CEMIP is the major hyaluronidase responsible for HA degradation in these cells.

CEMIP loss and inhibition suppresses fibroblast proliferation

The quantity and the molecular weight of hyaluronan associated with cells can impact on cell

proliferation [2,3]. We therefore examined whether CEMIP and its inhibition by sHA3.7 with subsequent accumulation of pericellular HA impacts on MEF proliferation. Treatment of MEFs with sHA3.7 dose-dependently and significantly reduced proliferation of the cells, in contrast to sHA1.2 or Delcore, which were inhibitory only at very high concentrations (Fig. 4A). Cell cycle analysis by flow cytometry confirmed that cells enter G1 arrest in response to sHA3.7 treatment, as reflected by an increased number of cells in G1 phase and a decreased fraction of cells in the subG1, S and G2/M phases (Supplementary Fig. 4). Consistently, genetic deletion of

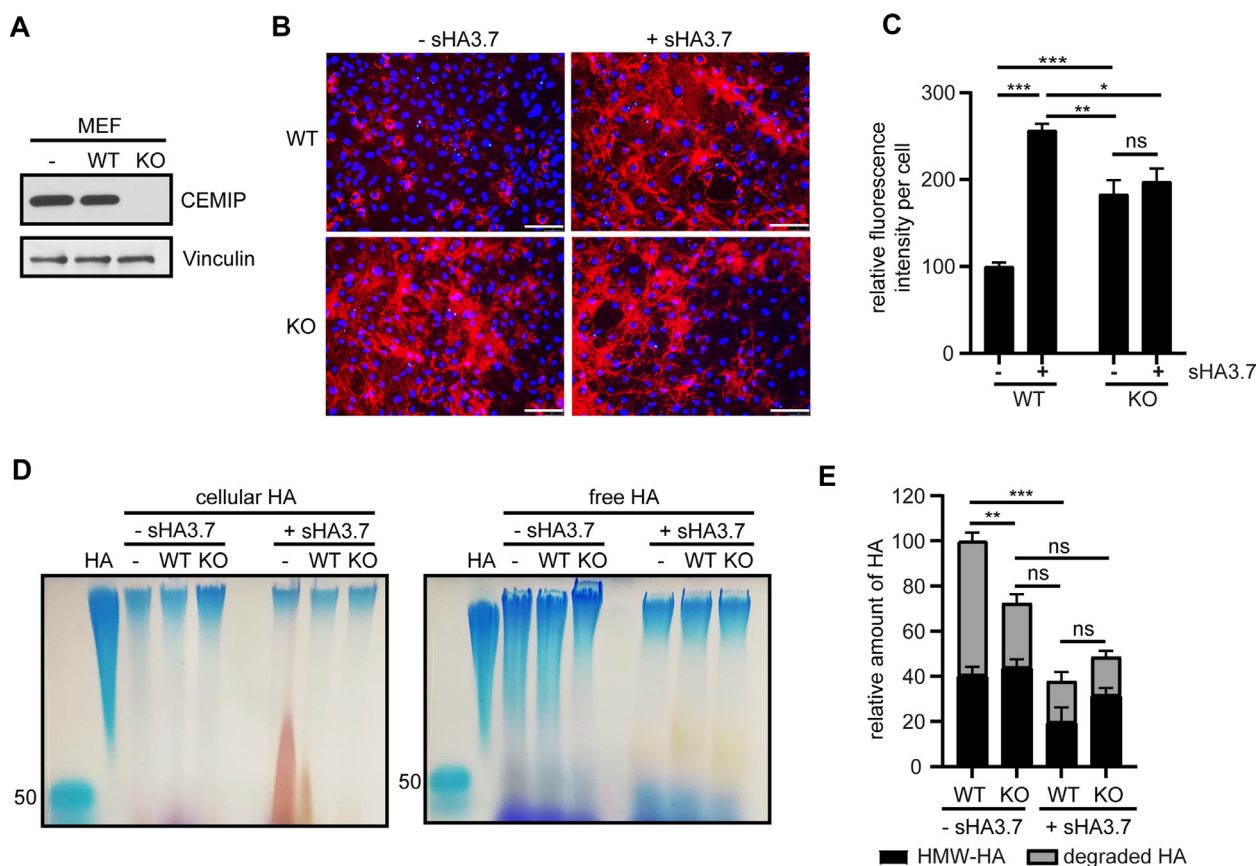


Fig. 3. Knockout of CEMIP and sulfated HA treatment influence HA metabolism of MEFs in a similar way. For all experiments, CEMIP WT and KO MEFs were used. To generate the cells, MEFs from transgenic mice harboring a floxed CEMIP gene (CEMIP^{flox/flox} MEFs) were transduced with adenoviral vectors expressing Cre recombinase or control constructs. **(A)** Western Blot analysis showed that after Cre expression, CEMIP expression is lost (KO). Cells transduced with control plasmids (WT) or untransduced cells (-) are shown as controls. **(B)** Treatment with sHA3.7 and loss of CEMIP increases the amount of pericellular HA. WT or KO MEFs were cultivated in chamber slides and were treated for 72 hours with or without 0.1 μ M sHA3.7. HA was detected with a biotinylated HABP and fluorescently labelled streptavidin. Representative images are shown. Scale bar 100 μ M. **(C)** HABP staining intensity was quantified in 8 images per condition. The data represent the mean \pm SE (n=8). Groups were compared using one-way ANOVA. *p < 0.05; **p < 0.005; ***p < 0.001; ns: not significant. **(D)** Treatment with sHA3.7 or loss of CEMIP increases the size of HA in the conditioned medium of fibroblasts. MEFs were cultivated for 4 days with 0.1 μ M sHA3.7 or were left untreated. HA was then purified from the cells and the conditioned media, analyzed by agarose gel electrophoresis and stained with Stains-All. HMW-HA (1.5 MDa) and 50 kDa HA fragments were used as size standards. For all panels, representative results from at least 3 independent experiments are shown. **(E)** Quantification of free HA levels. The amount of HA in each lane was quantified. HMW-HA was defined as the upper 25% of each lane, the lower 75% were considered to be degraded HA. The data represent the mean \pm SE (n=3). Significant differences for degraded HA are shown (one-way ANOVA. **p < 0.005; ***p < 0.001; ns: not significant).

CEMIP in MEFs also significantly reduced proliferation, to an extent comparable to that observed upon sHA3.7 treatment (Fig. 4B).

Pericellular HA plays a role in mediating contact inhibition [41]. In further experiments we therefore investigated whether the inhibition of MEF proliferation after sHA3.7 treatment or loss of CEMIP is dependent on the pericellular HA accumulation we observed under these conditions. Indeed, when pericellular HA was removed by treatment with bovine testis hyaluronidase, cell numbers increased significantly and the inhibitory effect of sHA3.7 treatment

or the absence of CEMIP on cell proliferation was rescued (Fig. 4C and D).

Next, we assessed whether sHA3.7 also influences HA metabolism and proliferation in other types of fibroblasts. Primary human dermal fibroblasts (HDFs) and MRC5 human fetal lung fibroblasts were treated with either sHA1.2, sHA3.7 or unmodified HA as a control, then cell-associated as well as free HA in conditioned media was analyzed by agarose gel electrophoresis. In both types of fibroblast, sHA3.7 increased the levels of cellular HA, while dramatically reducing the amount of HA degradation

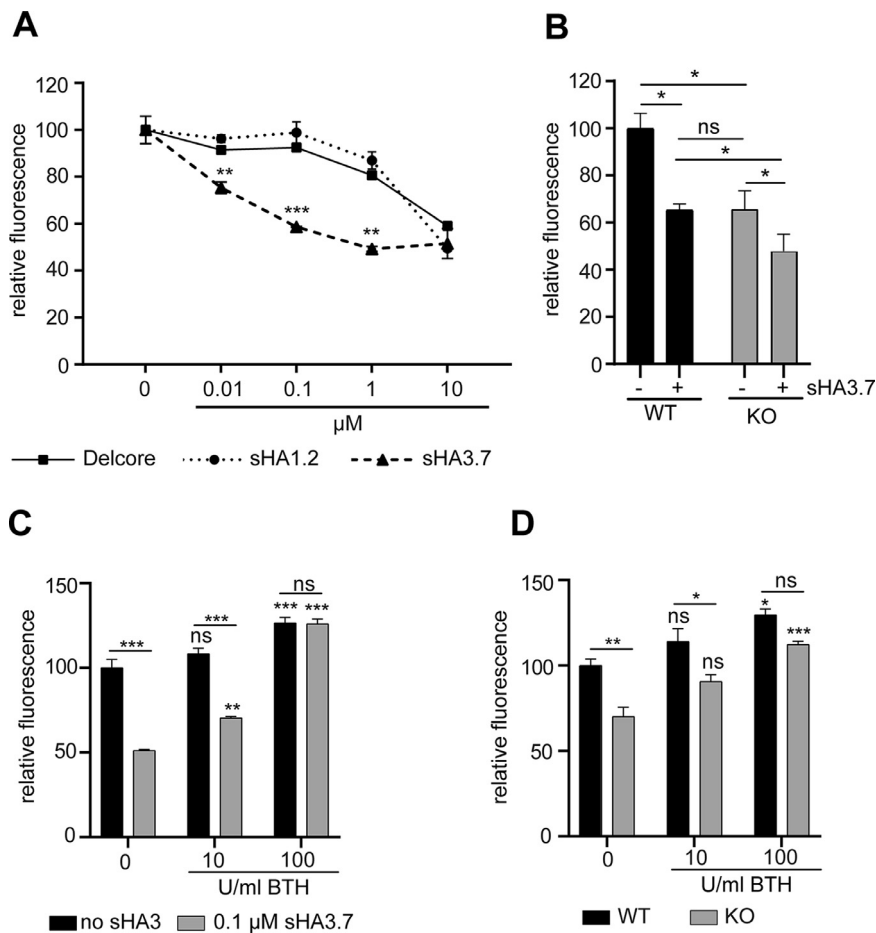


Fig. 4. Proliferation of MEFs is dependent on HA metabolism. **(A)** MEFs were treated with different concentrations of Delcore, sHA1.2 or sHA3.7 or were left untreated. **(B)** WT and CEMIP KO MEFs were treated with 0.1 μM sHA3.7 or were left untreated. **(C)** MEFs were treated with or without sHA3.7 and bovine testis hyaluronidase (BTH). **(D)** WT and KO MEFs were treated with or without BTH. In all experiments, 72 hours after the treatments indicated, the number of cells was quantified using the CyQUANT assay. Data represent means ± SE (n=3). One-way ANOVA: *p < 0.05; **p < 0.005; *** p < 0.001; ns: not significant. In (A) significant differences between Delcore and sHA3.7 treated samples are shown. In (C) and (D) unless otherwise marked, treated cells and the corresponding untreated controls (0) were compared.

products in the medium (Supplementary Fig. 5A and C). Similar to MEFs, sHA3.7 also significantly inhibited proliferation of HDFs and MRC5 cells (Supplementary Fig. 5B and D), indicating that this is a general effect of sHA3.7 on fibroblasts. To compare the effect of sHA3.7 with that of CEMIP loss, we performed siRNA knockdown experiments in MRC5 cells (Supplementary Fig. 5E). Again, we observed a similar change in HA levels and size in the CEMIP knockdown cells as with sHA3.7 treatment (Supplementary Fig. 5F). However, this effect was not as pronounced as that with the knockout MEFs, probably due to the transient nature of the knockdown. Furthermore, knockdown of CEMIP significantly inhibited MRC5 proliferation (Supplementary Fig. 5G). Treatment of the knockdown cells with sHA3.7 lead to only a limited further reduction of proliferation (Supplementary Fig. 5G), indicating that the

inhibitory effects of sHA3.7 on proliferation are mediated in the main by CEMIP.

Inhibition and loss of CEMIP promotes myofibroblast differentiation, but suppresses adipogenic and osteogenic differentiation

Recent studies have shown that the differentiation of resident fibroblasts into myofibroblasts, a process that is central to wound healing, is linked to HA metabolism, although the exact mechanism and the role of HA has not been elucidated [1,42]. Since our data demonstrated that CEMIP strongly influences HA metabolism in fibroblasts, we investigated whether CEMIP is involved in myofibroblast differentiation, and whether sHA3.7 can influence this process. TGFβ is a major inducer of fibroblast-to-myofibroblast differentiation [1,43]. Treatment of

cultivated MEFs with TGF β 1 induced a strong expression of α -smooth muscle actin (SMA) (Fig. 5A), a marker of differentiated myofibroblasts that is involved in cell motility and contractility during wound healing *in vivo*. This was associated with a marked reduction of CEMIP levels after TGF β treatment (Fig. 5A), in agreement with previous reports [7,11]. In CEMIP KO MEFs, SMA levels were higher at baseline and were more potently induced by TGF β than in WT MEFs (Fig. 5A), suggesting that CEMIP represses SMA expression. Consistently, we found that sHA3.7 treatment augmented TGF β -induced SMA expression in MEFs (Fig. 5B). Collectively, these data indicate that reduction of CEMIP levels or activity can promote myofibroblast differentiation.

Next, we investigated whether the loss of CEMIP in fibroblasts upon myofibroblast differentiation can also be observed *in vivo*. To this end, we employed co-staining of CEMIP with vimentin, a mesenchymal marker that is expressed in both fibroblasts and myofibroblasts [44], and examined the expression of CEMIP in fibroblasts in normal skin, as well as in the context of full-thickness skin wound healing where extensive myofibroblast differentiation takes place. In normal skin, strongest CEMIP expression was observed in papillary fibroblasts, but reticular fibroblasts were also CEMIP positive (Fig. 5C). During the proliferative phase of skin wound healing (3 - 8 days after wounding), dermal fibroblasts from the wound margins proliferate, migrate into the wounded area, become activated in response to factors such as TGF β , and differentiate into myofibroblasts as evidenced by increased SMA expression and extensive matrix deposition [43]. In sections of full-thickness wounds taken 7 days post-wounding, vimentin-positive CEMIP-expressing cells were readily detected, but the vast majority of SMA-positive myofibroblasts showed very little if any CEMIP staining (Fig. 5D and 5E). These data are consistent with our cell culture results, which indicate that CEMIP expression is downregulated upon myofibroblast differentiation.

Mesenchymal cells such as MEFs are multipotent cells that can differentiate into a number of lineages in addition to myofibroblasts, including adipocytes and osteoblasts. CEMIP has been reported to be involved in adipogenesis and bone development [17,45] and its expression has also been correlated with the degree of HA depolymerization in osteoarthritis and rheumatoid arthritis patients [11,19]. We therefore also investigated whether CEMIP plays a role in adipogenic and osteogenic differentiation of MEFs, and whether sHA3.7 can interfere with this. Upon induction of adipogenic differentiation, the expression levels of the adipogenic markers adiponectin, PPAR γ and CEBP α were significantly reduced in CEMIP KO MEFs compared to WT MEFs. Consistently, sHA3.7 treatment also

decreased adipogenic differentiation of WT MEFs, similar to the case with CEMIP KO MEFs, as evidenced by Oil Red O staining (Fig. 6A and B). Similarly, both loss of CEMIP and its inhibition by sHA3.7 treatment impaired osteogenic differentiation of the cells, as shown by reduced expression levels of the osteogenic markers BSP1, Osterix and Osteocalcin, and by von Kossa staining (Fig. 6C and 6D).

Collectively, these results indicate that sulfated HA derivatives inhibit CEMIP, which perturbs HA metabolism in fibroblasts. This has a pronounced effect on the differentiation capacity of fibroblasts, promoting their differentiation into myofibroblasts, while simultaneously suppressing adipogenic and osteogenic differentiation. Sulfated HA derivatives might therefore represent a potential tool for modulating normal or deregulated HA metabolism and fibroblast function in a range of physiological and pathophysiological settings.

Discussion

HA synthases and hyaluronidases coordinately regulate the concentration and the size of HA, which gives rise to specific HA microenvironments within tissues. The contribution of the hyaluronidase activity of CEMIP to the shaping of these HA microenvironments is poorly understood, in part due to a lack of inhibitors to study its function. Here we show that highly sulfated hyaluronic acid (sHA3.7) potently inhibits the CEMIP hyaluronidase activity. Focusing on CEMIP expression and activity in fibroblasts, which are the main producers of HA in the interstitial matrix, we found that sHA3.7 increased the pericellular levels of HMW-HA, decreased HA fragmentation, suppressed fibroblast proliferation, and fostered myofibroblast differentiation while inhibiting differentiation into the adipogenic and osteogenic lineages. The inhibitory effects of sHA3.7 were phenocopied by genetic loss of CEMIP expression. These data identify highly sulfated HA as an inhibitor of the CEMIP hyaluronidase activity that exhibits considerable selectivity over other hyaluronidases, and afford new insights into the role of CEMIP in regulating HA production by fibroblasts and in the determination of their differentiation fate.

Our studies show that highly sulfated HA is a potent inhibitor of CEMIP hyaluronidase activity in the low nanomolar range. Sulfated HA can also inhibit HYAL1, BTH and bee venom hyaluronidase [30], but much less potently. Of these, the hyaluronidase activity of HYAL1 shows the highest sensitivity to sulfated HA [30], yet we show here that the CEMIP hyaluronidase activity is more than an order of magnitude more sensitive to sulfated HA. Consistently, the effects we observed when CEMIP-expressing fibroblasts were treated with sulfated HA were also observed in fibroblasts in which CEMIP

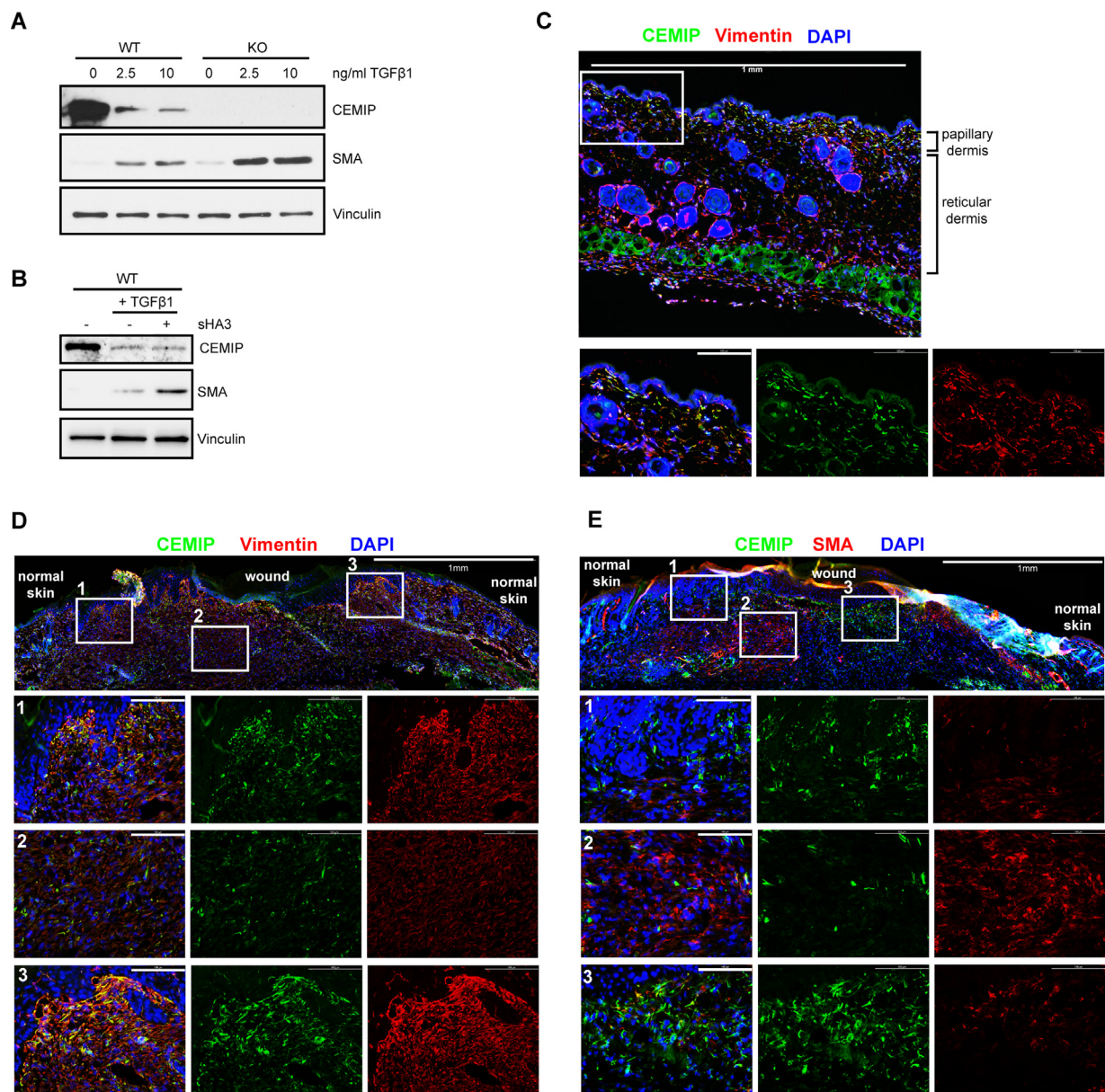


Fig. 5. CEMIP is expressed in vimentin-positive cells in skin and regulates SMA expression during TGF β -induced myofibroblast differentiation. **(A, B)** CEMIP WT and KO MEFs were starved and then treated for 24 hours with or without 2.5 or 10 ng/ml TGF β 1 **(A)** and with or without 2.5 ng/mL TGF β 1 and 0.1 μ M sHA3.7 **(B)**. The expression levels of CEMIP and SMA were analyzed by Western Blot. Vinculin served as loading control. **(C)** Sections from normal skin were stained for CEMIP (green) and vimentin (red). **(D, E)** Sections from punch biopsy wounds (7 days after wounding) were stained for CEMIP (green) and vimentin (red) **(E)** or CEMIP (green) and SMA (red) **(D)**. Scale bar: 1 mm in the lower magnification or 100 μ M in the higher magnification images.

expression was genetically abrogated. Several reports have employed sulfated HA as an inhibitor of HYAL1 [31,32]. In the light of our results, it is conceivable that at least a part of the effects observed in these studies may be due to inhibition of the CEMIP hyaluronidase activity. Further work will be needed to determine whether this is the case.

CEMIP-expressing cells have previously been shown to degrade exogenously added HA [7,11-13],

which we confirm here. In addition, we show that CEMIP is involved in the hydrolysis of endogenously produced HA, both in human and murine fibroblasts, which has a number of possible implications. First, chemical or genetic inhibition of CEMIP resulted in an accumulation of cell surface-associated HA. This may suggest that CEMIP is involved in the cleavage and release of freshly synthesized HA from the cell surface. Furthermore, our data indicate that this

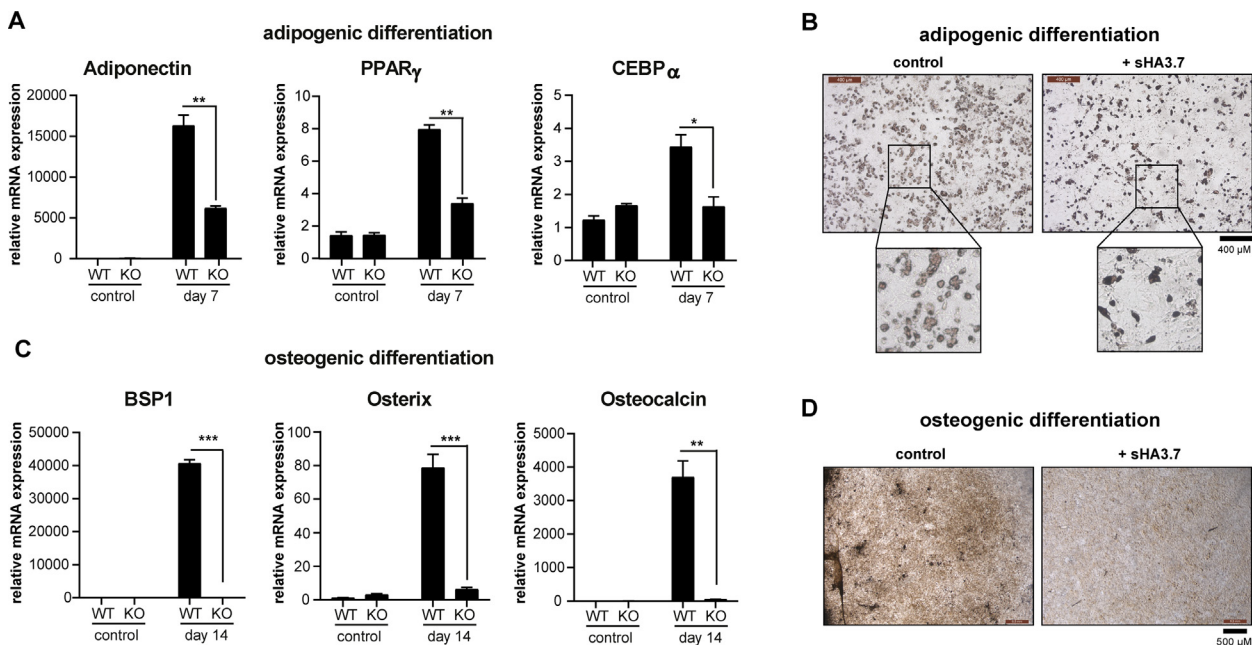


Fig. 6. Deletion or inhibition of CEMIP results in decreased adipogenic and osteogenic differentiation. **(A, B)** MEFs were differentiated into the adipogenic lineage. **(A)** Deletion of CEMIP reduces adipogenic differentiation. qPCR analysis of differentiated MEFs at day 0 (control) and day 7. Relative mRNA expression levels were analyzed for the adipogenic markers adiponectin, PPAR γ and C/EBP α and normalized to the housekeeping gene Rplp0. Data represent means \pm SE (n=3). Significance was calculated using the Student's t-test. *p < 0.05; **p < 0.005. The experiment was repeated three times independently and one representative example including triplicates for each condition is shown. **(B)** MEFs in the presence or absence of 0.1 μ M sHA3.7 were differentiated into the adipogenic lineage and stained with Oil Red O. Representative images of differentiated cells at day 7 of differentiation showing lipid-filled adipocytes. **(C, D)** MEFs were differentiated into the osteogenic lineage. **(C)** Deletion of CEMIP abrogates osteogenic differentiation. qPCR analysis of differentiated WT or KO MEFs at day 0 (control) and day 14. Relative mRNA expression levels were analyzed for the osteogenic markers bone sialoprotein (BSP1), osterix and osteocalcin and normalized to Rplp0 expression. Data represent means \pm SE (n=3). Significance was calculated using the Student's t-test. **p < 0.005; *** p < 0.001. The experiment was repeated three times independently. One representative example including triplicates for each condition is shown. **(D)** MEFs were differentiated into the osteogenic lineage in the presence or absence of 0.1 μ M sHA3.7 and stained for mineral deposition using von Kossa stain.

accumulation results in decreased proliferation of fibroblasts, consistent with the role of HMW-HA in the regulation of contact inhibition [41], and reminiscent of the early contact inhibition observed in naked mole rat fibroblasts that synthesize very high molecular weight HA due to expression of a species-specific isoform of HAS2 [46–48]. Second, our results also suggest that CEMIP contributes to the production of LMW-HA by fibroblasts, which accumulates under cell culture conditions *in vitro*. *In vivo*, increased CEMIP expression, as observed for example in different tumor entities and cells from osteoarthritis and rheumatoid arthritis patients [11,19-22,24], might lead to an accumulation of LMW-HA which contributes to a pro-angiogenic and pro-inflammatory environment [2,3].

Experiments with artificial extracellular matrices (aECM) composed of collagen I and sulfated HA showed that sulfated HA in this system promotes fibroblast adhesion and proliferation and also prevents TGF β 1-induced SMA expression, probably via modulation of the bioavailability of growth factors

[49,50], since sulfated HA derivatives can interact with growth factors such as TGF β 1, BMP-4 and VEGF-A [51–53]. In contrast, we found that sulfated HA inhibits fibroblast proliferation and fosters TGF β 1-induced SMA expression. These differences are likely concentration and/or conformation dependent. Notably, aECM is produced using a solution that contains 0.5 mg/ml sHA3.7 (equivalent to approximately 5 - 10 mM sHA3.7), which is then dried onto plastic to create a substrate for cell attachment and growth [54]. In contrast, we observed an inhibitory IC $_{50}$ for sHA3.7 in free solution on CEMIP hyaluronidase activity in the low nanomolar range.

Despite structural similarities to the sulfated HA used in this study, chondroitin-4-sulfate and chondroitin-6-sulfate did not inhibit the CEMIP hyaluronidase activity, although we did observe that both chondroitin sulfates inhibited bovine testis hyaluronidase (data not shown), as reported by others [38]. On the one hand, these data suggest that chondroitin sulfates *in vivo* do not play a role in regulating the

CEMIP hyaluronidase activity. On the other hand, despite a comparable degree of total sulfation at the same position as in sHA1.2, chondroitin-6-sulfate did not inhibit the hyaluronidase activity of CEMIP, indicating that not only the sulfation but also the sugar backbone is critical for inhibition of the CEMIP hyaluronidase activity. The stereoisomeric difference between the sulfated glycosaminoglycans thus might be responsible for the different potency of CEMIP inhibition, which is also in line with the observation that CEMIP does not bind to or degrade chondroitin sulfate [7].

HA has been implicated in all steps of wound healing and is generally thought to promote it, although many aspects of this dynamic process are still insufficiently understood. A crucial step during wound healing is the differentiation of fibroblasts into myofibroblasts induced by TGF β , which is intimately linked to and regulated by hyaluronan levels. HA accumulates pericellularly during myofibroblast differentiation through reduced HA turnover [39], which facilitates TGF β -induced fibroblast proliferation [42] and myofibroblast differentiation [55]. Our data and those of other groups [7,11] show that CEMIP is down-regulated after TGF β stimulation. Based on our findings that both sHA3.7-treated and CEMIP knock-out fibroblasts exhibited augmented TGF β -induced SMA expression, we propose that the loss of CEMIP upon exposure to TGF β is responsible for increased pericellular HA levels, which fosters myofibroblast differentiation. Consistent with this notion, CEMIP is expressed in vimentin-positive fibroblasts in both normal skin and full-thickness skin wounds, but myofibroblasts in the proliferative phase of cutaneous wound healing did not exhibit any significant CEMIP expression. In line with these results, hydrogels releasing highly sulfated HA accelerate wound healing, as reflected in increased SMA positive granulation tissue in the wounds [56].

Our results show that treatment with sulfated HA and loss of CEMIP is associated with increased pericellular levels of HA, and inhibits the differentiation of fibroblasts into the adipogenic and osteogenic lineages. These data are consistent with the observation that HA fosters mesenchymal stem cell quiescence and maintains their differentiation potential [57], and that HA plays an inhibitory role in adipogenesis [45]. Similarly, hematopoietic stem cells produce HA, which suppresses their proliferation and differentiation [58]. Our data showing that inhibition or loss of CEMIP suppresses osteogenic differentiation are also consistent with results obtained in mice with genetic deletion of CEMIP, in which lengthening of the hypertrophic zone in the growth plate, accumulation of HMW-HA within the hypertrophic zone, and shortening of the long bones were observed [17]. In conjunction with our data showing that perturbation of HA turnover in fibroblasts through sHA3.7-mediated inhibition of the CEMIP

hyaluronidase activity fosters myofibroblast differentiation, these observations implicate CEMIP-dependent HA degradation as a key regulator of mesenchymal progenitor cell differentiation.

Modulation of hyaluronan levels and its metabolism has a number of potential therapeutic applications. Application of exogenous HA is already used to improve wound healing [59], and intra-articular injection of HMW-HA can be employed to increase HA levels for the treatment of osteoarthritis [60]. Our results suggest that inhibition of CEMIP through treatment with sulfated HA would be expected to increase HMW-HA levels, which could have a similar therapeutic effect in these contexts. In this regard, we note that sulfated HA is well tolerated *in vivo* [31,32,56]. Our results also suggest that sulfated HA should reduce the amount of LMW-HA, thereby attenuating the inflammation induced by small HA oligosaccharides. This may be particularly relevant in the context of rheumatoid arthritis and osteoarthritis, in which increased accumulation of HA degradation products in the synovial fluid is associated with inflammation and disease progression [61]. Interestingly, CEMIP is overexpressed in chondrocytes and synovial fibroblasts from osteoarthritis patients and is responsible for their HA degrading activity [11,16,18,19]. Inefficient downregulation of CEMIP by TGF β in arthritic synovial fibroblasts is linked to the accumulation of depolymerized HA in patients suffering from rheumatoid arthritis and osteoarthritis [11], lending further credence to the notion that inhibition of the CEMIP hyaluronidase activity through sulfated HA might represent a promising new treatment option for these diseases.

Experimental procedures

Ethics statement

All mice were maintained in accordance with German government and institutional guidelines and regulations. Permission for the experiments in this study was granted by the local authorities (Permit numbers TVV24/12). Embryos were sacrificed by decapitation. The completely anonymized human dermal fibroblast strain GS4 was established prior to the Human Tissue Act 2004 by outgrowth of explants taken from surplus tissue obtained during surgical reduction mammoplasty (breast reduction) on healthy donors younger than 40 years of age. They were originally obtained from Dr. J.H. Peacock, Institute of Cancer Research, Sutton, UK. For a detailed description, see [62] and references therein.

Cell culture

293T cells were cultivated at 37°C in DMEM, 10% FCS, 1% penicillin-streptomycin. Primary MEFs

were isolated from E13.5 embryos of C57Bl/6 of FVB mice as previously described [63]. Briefly, the head and organs were removed and embryos were minced and incubated in trypsin overnight at 4°C. The next day, the trypsin was removed and the tissue was incubated for 20 min at 37°C. Then, cells were resuspended in DMEM supplemented with 10% heat-inactivated FCS, 1% penicillin-streptomycin and 2 mM L-glutamine and plated. MRC5 cells (human fetal lung fibroblasts) were a kind gift from Thordur Oskarsson, DKFZ and were cultivated in MEM, 10% FCS, 2 mM glutamine, 1% non-essential amino acids, 1% penicillin-streptomycin. Primary human dermal fibroblasts were cultivated in DMEM, 10% FCS, 1% penicillin-streptomycin. MEFs and human dermal fibroblasts were cultivated at 37°C, 5% CO₂, 5% O₂. 293T and MRC5 cells were cultivated at 37°C, 5% CO₂, 21% O₂.

Plasmids and transfection

293T cells were transfected with HYAL1 or CEMIP expression vectors or controls using Lipofectamine 2000. The murine HYAL1 sequence was cloned into the pEF6/V5-His-Topo vector (Life Technologies) as previously described [64]. The following primers were used: 5'-GGC CAA GAC ATG CTT GGG C-3' and 5'-GTG TGC AGT TGG GTG CAG C-3'. Plasmids containing the murine or human cDNA sequence of CEMIP in the pRP vector were purchased from VectorBuilder (vector ID murine CEMIP: VB180316-1177crn; vector ID human CEMIP: VB191004-1084jkc; vector ID empty vector control: VB171110-1101tcx). Expression of HYAL1 and CEMIP was monitored by immunoblotting and by analyzing HA degradation. For most experiments transiently transfected cells were used. 293T cells stably transfected with CEMIP were generated by selection with puromycin.

siRNA-mediated CEMIP knockdown in MRC5 cells

ON-TARGET plus CEMIP siRNA (si CEMIP) and the corresponding ON-TARGET plus Non-targeting Pool (si NT) were purchased from Dharmacon (L-022291-00-0005 and D-001810-10-05). Transfections were performed with Lipofectamine RNAiMAX (Thermo Fisher Scientific) according to the manufacturer's instructions. Knockdown of CEMIP was monitored by Western Blot analysis.

Knock-out of CEMIP in MEFs

For inactivation of CEMIP, transgenic mice on a mixed C57Bl6/FVB background harboring two loxP sites flanking exon 3 and 4 of the CEMIP gene (CEMIP^{fllox/fllox}) were used, which were kindly provided by Marcus Möller (RWTH Aachen) and generated by

Alain Chariot (University of Liège) [40]. The mice were genotyped by PCR using the following primer sequences: For: TGGTACACATGTCACATGGTAGAC; Rev: GACAACAATAACCATATGCCTAGG. MEFs isolated from transgenic mice were transduced with adenoviral constructs expressing Cre recombinase followed by an IRES-EGFP or the respective EGFP control constructs with a MOI of 500. Constructs were purchased from VectorBuilder (Vector ID pAV-CMV-Cre-IRES-EGFP: VB190509-1062zan and pAV-CMV-EGFP VB150925-10024). Efficient knock-out of CEMIP was confirmed by Western Blot analysis.

Glycosaminoglycans

High molecular weight HA (HMW-HA) was from Abbott Medical Optics (Healon5) or from Lifecore Biomedical (1.5 MDa). Hyaluronan with a molecular weight of 50 kDa (Select-HA) was from Hyalose. For preparation of 10 kDa HA fragments, Healon was digested for 6 hours with 100 U/ml BTH with subsequent centrifugation through Amicon ultracentrifugal filters with a molecular-weight cut-off of 10 kDa (Millipore). Delcote (Contipro) is hyaluronic acid chemically modified by oleic acid and served as a control for modified HA. Chondroitin-4-sulfate (chondroitin sulfate A) from bovine trachea and chondroitin 6-sulfate from shark cartilage (90%) were both obtained from Sigma-Aldrich.

Preparation and characterization of sulfated hyaluronan

Sulfated HA derivatives were synthesized by INNOVENT e.V. using high-molecular weight HA obtained from either Aqua Biochem (*Streptococcus* sp., Mw 1.1×10^6 gmol⁻¹) or from Kraeber (Mw 9.3×10^5 gmol⁻¹). The synthesis of sulfated GAG derivatives has been described previously [50-52,65-67]. Sulfur trioxide/dimethylformamide complex (SO₃-DMF, 47% active SO₃) and sulfur trioxide/pyridine complex (SO₃-pyridine, active SO₃ ~ 48-50% pract., ≥ 45% SO₃) were obtained from Fisher Scientific (Schwerte, Germany). For preparation of the low-sulfated HA derivative sHA1.2, SO₃-pyridine was used as a sulfation reagent in a ratio of polymeric OH-group/SO₃ of 1: 3.5. The reaction time was 20 min at room temperature. The sulfation reagent for the preparation of high-sulfated HA derivatives sHA3.4, sHA3.5, sHA3.6 and sHA3.7-1 was SO₃-DMF, with a ratio of polymeric OH-group/SO₃ of 1: 20 and a reaction time of one hour. For the sHA3.7-2 we used SO₃-pyridine in a ratio of polymeric OH-group/SO₃ of 1: 15. The sHA2.0 and sHA2.5 were prepared with both sulfation reagents. Polymers were purified by dialysis, first against aqueous 0.025 M NaHCO₃-solution and subsequently against de-ionized water, followed by freeze-drying under a high vacuum. The respective

degree of sulfation (D.S.) of the sulfated GAG derivatives was determined by elemental analysis. The molecular weight and the dispersity ($D = M_w/M_n$) was estimated by gel permeation chromatography (GPC) equipped with laser light scattering-, refraction index- and UV-detection [66]. The sulfate group distributions within the repeating disaccharide unit of the GAG were detected by high-resolution ^{13}C nuclear magnetic resonance [52,68]. Supplementary Fig. 6 and Supplementary Table 1 summarize the properties of the sulfated hyaluronan preparations used in this study.

HA degradation by hyaluronidases

Hyaluronidase activity of bovine testis hyaluronidase (BTH, Sigma Aldrich) was analyzed in 0.3 M sodium phosphate buffer pH 5.3 and incubated for 16 hours at 37°C with HA, sulfated HA and controls. For HYAL1 activity assays, 293T cells transfected with a pEF-HYAL1 plasmid or vector control were cultivated in serum-free medium for 48 hours. The conditioned media containing secreted HYAL1 were collected and used directly or stored at -80°C. Conditioned medium (10-30 μl) was diluted in 0.3 M sodium acetate buffer pH 3.7 in a reaction volume of 100 μl and incubated with 20 μg HA, with or without sulfated HA and controls for 16 hours at 37°C. Subsequently HA in the reactions was precipitated with 4 volumes of ethanol by incubation at -20°C. Samples were then centrifuged at 10000 g for 10 min, pellets were washed with 70°C ethanol, dried, resuspended in H_2O and analyzed by agarose gel electrophoresis.

CEMIP hyaluronidase activity was assessed with cells in culture, similar to assays described recently [7]. 293T cells were transfected with vectors containing mouse or human CEMIP cDNA or empty vector controls and reseeded 16 hours after transfection in 24 well plates at 80000 cells / well. After cells had adhered, 100 $\mu\text{g}/\text{ml}$ HA was added in a total volume of 500 μl . After 72 hours, medium was collected, 1/10 volume Proteinase K (1 mg/ml in 100 mM ammonium acetate, 0.1% SDS) was added and incubated at 60°C for 4 hours. HA was precipitated with 4 volumes ethanol by incubation at -20°C overnight. Samples were then centrifuged at 10000 g for 10 min, pellets were washed with 70% ethanol and after drying resuspended in H_2O for analysis by gel electrophoresis. The data used for the graphs (CEMIP and HYAL1) are derived from three independent experiments with one sample per condition each.

Analysis of HA degradation products

Electrophoresis of HA was performed according to a protocol provided by Cleveland Clinic (NHLBI award number PO1HL107147), which is based on

the method of Lee and Cowman [69]. Hyaluronan samples were mixed with Bromophenol Blue loading buffer and analyzed by gel electrophoresis using 1% agarose (Biozym Scientific) in TAE buffer (40 mM Tris, 20 mM glacial acetic acid, 1 mM EDTA, pH 8.0). Immediately after the run, the gel was placed in 30% ethanol for 1 hour on a shaker. Subsequently the gel was stained overnight under a light-protective cover in 2.5 $\mu\text{g}/\text{ml}$ Stains-All (Sigma-Aldrich) in 30% ethanol. For destaining, the gel was transferred to H_2O and incubated for several hours in the dark. The gel was then placed on a light box for several minutes to complete the destaining and then photographed. Healon (5 MDa) or 1.5 MDa HA as well as 10 and 50 kDa HA served as size standards.

HABP staining of cells

Cells were plated on glass or plastic chamber slides, cultivated in DMEM supplemented with 10% heat-inactivated FCS, 1% penicillin-streptomycin and 2 mM L-glutamine and treated with the indicated concentrations of sHA1.2, sHA3.7 or Delcore and incubated for 72 hours. For HABP staining, cells were fixed with 3.7% formaldehyde, 70% ethanol, and 5% glacial acetic acid (all v/v) for 15 min at room temperature and subsequently air-dried. Cells were washed three times with PBS. Blocking was performed using 3% BSA (biotin-free) in PBS for 1 hour at room temperature. Hyaluronan was stained with hyaluronic acid binding protein (HABP, Calbiochem #385911, 2.5 $\mu\text{g}/\text{ml}$) in 3% BSA overnight at 4°C. Cells were washed three times with PBS, and bound HABP was detected using Alexa Fluor 546-labelled streptavidin (5 $\mu\text{g}/\text{ml}$) at room temperature for 1 hour. Cells were washed three times with PBS and stained with DAPI (0.5 $\mu\text{g}/\text{ml}$ for 5 min). Slides were mounted with Fluoromount. Immunofluorescence images were acquired using a Leica DM5500 microscope and a 20x objective (Leica). Total HABP staining signal (integrated density) was measured in 6 to 8 randomly selected fields from the same well per condition using ImageJ. The mean signal of fields stained with Alexa Fluor 546-labelled streptavidin only (background) was subtracted, and the numbers were normalized to the mean value for the untreated cells, which was set to 100%.

HA purification

Purification and analysis of HA from cells and conditioned media of cells was performed according to a protocol provided by Cleveland Clinic (NHLBI award number PO1HL107147). Cells were cultivated for 3 to 4 days with or without sulfated HA. Media were collected and incubated for 4 hours at 60°C with 100 $\mu\text{g}/\text{ml}$ Proteinase K (Roth). Cells were harvested with 100 $\mu\text{g}/\text{ml}$ Proteinase K and also incubated at 60°C. Insoluble material was removed by

centrifugation (5000 rpm, 10 min). Samples were then mixed with 4 volumes ethanol, incubated overnight at -20°C and centrifuged at 10000 g for 10 minutes. The pellet was washed with 4 volumes 70% ethanol, centrifuged again, air-dried and resuspended in 100 μ l 100 mM ammonium acetate. To inactivate Proteinase K, samples were incubated 5 minutes at 95°C. To normalize the amount of sample used, DNA content was measured using CyQuant NF (Thermo Fisher Scientific) and equal amounts were then used for further steps. Nucleic acids were digested at 37°C after adding 6 U of DNase (Promega) and 4 μ g RNase (Thermo Fisher Scientific). Enzymes were inactivated for 5 minutes at 95°C, insoluble material was removed by centrifugation (5000 g 10 minutes 4°C) and HA was precipitated with 4 volumes of ethanol. After incubation at -20°C, samples were centrifuged again at 10000 g for 10 minutes, the pellets were washed with 70% ethanol, air-dried and resuspended in H₂O. Samples were then analyzed by agarose gel electrophoresis and staining with Stains-All.

Quantitative analysis of hyaluronan agarose gels

ImageJ [70] was used to calculate intensities of HA levels in hyaluronan agarose gels stained with Stains-All. To reduce unspecific signals, for example the brown bands derived from sHA3.7 on the gels, a colour deconvolution filter (Fast Red Fast Blue DAB) [71,72] was applied to the images and the image with the strongest signal was used for further steps. After inverting the image, plot profiles were measured in each lane by using the line selection tool and an appropriate line width. From the resulting intensities the minimum grey value of the picture was subtracted to reduce the background signal. The integrated density was calculated by adding up all intensity values in each lane to quantify the total HA values in each lane. For calculation of a dose response curve and IC₅₀ values (Fig. 1) the gravity of the curve was calculated at 50% of the total HA amount in each lane. The resulting values were used for normalization, whereby digested HA without inhibitor was set to 0% and undigested HA was set to 100% inhibition. These data were used to calculate a four-parameter dose-response curve using non-linear regression (curve fit) with GraphPad Prism. To monitor a shift in the size of HA (Fig. 3) the integrated intensity in four equal regions (quartiles Q1 to Q4) within each lane was calculated. (Q1: HMW-HA, Q2-Q4: degraded HA). The quantifications represent data from three independent experiments with one sample per condition each.

Western Blot

Cells were lysed in 50 mM Tris-HCl pH 7.5, 150 mM NaCl, 1 mM EDTA, 1% NP-40, 0.5%

sodium desoxycholate, 0.1% SDS supplemented with protease inhibitor mix (Roche) and clarified by centrifugation (15 min 13000 rpm). Total protein concentration was measured using BCA assays. Samples were diluted in sample buffer (final concentration 62.5 mM Tris-HCl pH 6.8, 2% SDS, 10% glycerol, 0.005% bromophenol blue and freshly added DTT (100 mM)). The samples were subjected to SDS-PAGE and transferred to Immobilon-P PVDF membrane (Merck Millipore) by using standard Western Blotting techniques. The membranes were probed with polyclonal anti-CEMIP (ab 98947, Abcam or ARP42526 P050, Avivasystems), anti-SMA (A2547, Sigma) or anti-vinculin (V9131, Sigma) antibodies. HRP-conjugated secondary antibodies were from DAKO. The protein bands were visualized using the Pierce ECL or ECL Dura Western Blotting Substrate (Thermo Fisher Scientific).

Proliferation assays

The CyQuant NF Cell proliferation assay Kit (Thermo Fisher Scientific) was used to assess cell numbers. Cells were seeded into 96-well plates at a density of 1×10^3 cells per well and cultivated overnight. Cells were then stimulated for 72 h with the indicated concentrations of sHA1.2, sHA3.7, Delcore, BTH, LMW-HA or HMW-HA (Healon5). After cultivation, cells were incubated with 50 μ l CyQuant Dye Binding Solution at 37°C for 30 minutes. The fluorescence intensity of each well was measured with excitation at 480 nm and emission at 530 nm with a SpectraMax iD3 microplate reader (Molecular Devices). Quantifications are based on triplicates derived from separate wells.

Flow Cytometry

Flow Cytometry was used to analyze cells in different phases of the cell cycle. MEFs were treated for 3 days with 0.1 μ M sHA1.2, sHA3.7 or Delcore or were left untreated. Adherent and floating cells were harvested and fixed in 70% ice-cold ethanol. After fixation cells were washed once in PBS, stained with DRAQ5 (Biostatus Ltd) and analyzed with a FACScan flow cytometer and Cell Quest Pro software (Becton Dickinson). Quantifications are based on triplicates derived from separate dishes.

Myofibroblast differentiation of MEFs

CEMIP WT and KO MEFs were starved for 48 hours in DMEM, 0.1 % FCS (heat-inactivated), 2 mM glutamine, then treated with or without 2.5 or 10 ng/ml TGF β 1 (Peprotech) and 0.1 μ M sHA3.7 in starvation medium. Cells were harvested after 24 hours for Western Blot analysis.

Osteogenic and adipogenic differentiation of MEFs

Differentiation experiments were performed with MEFs of passage 2-4. For osteogenic differentiation, cells were plated at 2×10^4 cells/cm² and treated with 50 µg/ml ascorbic acid (Sigma 49752), 10 mM β-glycerophosphate (Sigma G9422) and 200 ng/ml BMP2 (Peprotech, # P12643). Cells were incubated with this differentiation cocktail over a period of 14 days with medium changes every 3 to 4 days. RNA was harvested at the indicated time points. After 14 days of differentiation, cells were fixed in formalin prior to staining with von Kossa stain. For adipogenic differentiation, cells were plated at high density (3.5×10^4 cells/cm²) and grown to post-confluency. After 5-7 days, cells were induced to differentiate with 5 µg/ml insulin, 0.5 µM 3-isobutyl-1-methylxanthine (IBMX), 1 µM dexamethasone and 10 µM troglitazone (all from Sigma) for three days. Then, cells were incubated with maintenance medium containing 5 µg/ml insulin for two days. Medium was changed to normal growth medium for two additional days. RNA was harvested at the indicated time points or cells were stained with Oil Red O.

Histological staining of cells

Mineral deposition was evaluated by von Kossa staining. Formalin-fixed cells were incubated with 5% AgNO₃ for 15 minutes followed by 5 minutes of 1% pyrogallol. After fixation with 5% sodium thiosulfate solution, cells were rinsed with H₂O and images were taken. Lipid droplet formation was assessed by Oil Red O staining. Formalin-fixed cells were rinsed in 60% isopropanol for 2 minutes. Subsequently, cells were incubated for 30 minutes in Oil Red O staining solution (Sigma) prepared following the manufacturer's instructions, then rinsed with H₂O before images were acquired.

RNA isolation and Reverse transcription PCR (RT-PCR)

Total RNA was isolated from the cells using TRIzol (Invitrogen) according to the manufacturer's instructions. RNA (5 µg) was digested by 5 U DNase I (Thermo Fisher Scientific) at 37°C for 30 minutes. The reaction was stopped by addition of EDTA and heat inactivation, then the RNA was transcribed into cDNA using reverse transcriptase and random primers (both from Thermo Fisher Scientific) according to the manufacturer's protocol. Gene expression was analyzed using SYBR-Green mix (Applied Biosciences) to perform real-time qPCR using the Mx3005P QPCR System (Agilent). The sequences of primers used for qRT-PCR analysis are listed below. Rplp0 mRNA transcripts served as an

internal (housekeeping) control. Relative quantitative analysis was performed using the $2^{-\Delta\Delta Ct}$ method. Quantifications are based on triplicates derived from separate wells.

Rplp0 For GGACCCGAGAAGACCTCCTT; Rplp0 Rev GCACATCACTCAGAATTTCAATGG; Pparγ For GGGGTGATGTGTTTGAACCTTG; Pparγ Rev CAGGAAAGACAACAGACAAAT; Adiponectin For CCTGGCCACTTTCTCCTCATT; Adiponectin Rev ACAGGAGAGCTTGCAACAGT; CEBPα For GTGCTGGAGTTGACCAGTGA; CEBPα Rev AAACCATCCTCTGGGTCTCC; BSP For CCAGGACTGCCGAAAGGAAG; BSP Rev CCCCCTTTTCTTCAGAATCCTCTG; Osteocalcin For CTGACAAAGCCTTCATGTCCA; Osteocalcin Rev GCGCCGGAGTCTGTTCATA; Osterix For AGCGACCACTTGAGCAAACAT; Osterix Rev: GCGGCTGATTGGCTTCTTCT

Generation of wounds in mice

Wound healing studies were performed according to institutional and state guidelines and were approved by the Committee on Animal Welfare of Saxony (Germany, TVV24/12). Wounds were inflicted in 10 to 12 weeks old C57BL/6 mice under anesthesia as previously described [73]. The back of the mice was shaved and two full-thickness wounds (including panniculus carnosus) were created with a 6-mm dermal biopsy punch on both sites of the back. Wounds were harvested at day 7 post wounding by excising the original wound tissue using surgical instruments, which was then deep-frozen in Tissue Freezing Medium™. For immunostaining, 6 µm thick tissue sections were prepared.

Immunofluorescence on tissue sections

Sections were fixed in acetone for 10 minutes on ice and air-dried. For CEMIP and vimentin double stainings, tissue sections were blocked in 10% goat serum in PBS for 1 hour at room temperature in a humidified chamber. Sections were stained with 5 µg/ml CEMIP antibody (rabbit, ab98947, Abcam) and 10 µg/ml vimentin antibody (chicken, Biolegend, 919101) in 10% goat serum over night at 4°C. After washing 3 times with PBS, sections were incubated with secondary antibodies (1.5 µg/ml goat anti-rabbit Alexa 488 and 1.5 µg/ml goat anti-chicken, DyLight 550) in 10% goat serum for 1 hour at room temperature. Sections were then washed 3 times in PBS, stained with DAPI (1 µg/ml in water) and embedded using fluorescence mounting medium (Dako). For double staining of CEMIP with SMA the MOM Kit (Vector Labs) was used. Tissue sections were blocked with Avidin-Biotin blocking kits (Vector Labs) followed by incubation in 10 % goat serum in PBS for 1 hour at room temperature in a humidified chamber. Sections were stained with 5 µg/ml

CEMIP antibody (polyclonal rabbit anti-CEMIP, ab98947, Abcam) in 10% goat serum and MOM blocking reagent over night at 4°C. Sections were washed twice with PBS and incubated for 5 min with Diluent working solution (MOM Kit). Sections were then incubated with SMA antibodies (A2547, ascites fluid, diluted 1:1000, Sigma) in Diluent working solution (MOM Kit) for 30 min at room temperature. After washing twice in PBS, a biotinylated anti-mouse IgG (MOM Kit) was applied for 10 minutes at room temperature, followed by two further washes with PBS and incubation with secondary antibodies (1.5 µg/ml goat-anti-rabbit Alexa 488) and streptavidin-546 (5 µg/ml) for 30 minutes at room temperature. Sections were then washed 3 times in PBS, stained with DAPI (1 µg/ml in water) and embedded using fluorescence mounting medium (Dako). Immunofluorescence images were acquired using a Leica DMI8 microscope (Leica).

Statistical analysis

Comparison between two groups was performed using a two-tailed Student's t-test. For comparing more than two groups within the same experiment, one-way ANOVA was used in GraphPad Prism (version 9). Unless otherwise stated, all experiments were repeated independently three times with equivalent results. One representative example, with replicates for each condition, is shown. Statistical significance was set at $p < 0.05$. Data are expressed as mean \pm SE. (* $p < 0.05$, ** $p < 0.005$, *** $p < 0.001$).

Funding

JPS is the “Franz-Volhard-Stiftungsprofessur für Mikrovaskuläre Biologie und Pathobiologie”, which was funded by the Klinikum Mannheim GmbH during part of this work. AS was funded by the “Brigitte-Schlieben-Lange-Programm” of the Ministerium für Wissenschaft, Forschung und Kunst Baden-Württemberg. SF and UA received funding from the German Research Council (Deutsche Forschungsgemeinschaft, DFG) (project number 59307082—SFB-TRR67 - subprojects B3 to SF and B4 to UA), the European Regional Development Fund (project number 100052718 to UA) and from the German Research Council (project FR2671/4-1 to SF). SM and MS gratefully acknowledge financial support by the German Research Council (DFG SFB/Transregio 67, project Z3).

Author contributions

Anja Schmaus: Conceptualization, Methodology, Formal analysis, Investigation, Writing - Original Draft, Writing - Review & Editing, Visualization

Melanie Rothley: Methodology, Investigation
Caroline Schreiber: Methodology, Investigation
Stephanie Möller: Methodology, Resources
Sven Roßwag: Investigation
Sandra Franz: Investigation, Resources
Boyan K. Garvalov: Formal analysis, Visualization, Writing - Review & Editing
Wilko Thiele: Investigation, Writing - Review & Editing
Sofia Spataro: Resources, Investigation
Carsten Herskind: Resources
Marco Prunotto: Resources, Supervision
Ulf Anderegg: Resources, Project administration
Matthias Schnabelrauch: Resources, Project administration
Jonathan Sleeman: Conceptualization, Writing - Original Draft, Writing - Review & Editing, Supervision, Project administration, Funding acquisition

Acknowledgments

The authors gratefully acknowledge the excellent technical assistance of Amra Noa, as well as the assistance and expertise of Sabine Müller and Selma Huber with the animal husbandry.

Keywords:

Hyaluronan (HA);
hyaluronidase;
CEMIP;
KIAA1199;
fibroblast;
sulfated HA

Abbreviations:

HA, hyaluronan (hyaluronic acid); HMW-HA, high molecular weight hyaluronan; sHA, sulfated HA; LMW-HA, low molecular weight hyaluronan; MEF, mouse embryonic fibroblasts; HDF, human dermal fibroblasts; aECM, artificial extracellular matrix

References

- [1] S. Albeiroti, A. Soroosh, C.A. de la Motte, Hyaluronan's role in fibrosis: a pathogenic factor or a passive player? *BioMed Res. Int.* 2015 (2015) 790203, doi: [10.1155/2015/790203](https://doi.org/10.1155/2015/790203).
- [2] T. Kobayashi, T. Chanmee, N. Itano, Hyaluronan: metabolism and function, *Biomolecules* 10 (2020), doi: [10.3390/biom10111525](https://doi.org/10.3390/biom10111525).
- [3] A. Schmaus, J. Bauer, J.P. Sleeman, Sugars in the microenvironment: the sticky problem of HA turnover in tumors, *Cancer Metastasis. Rev.* 33 (2014) 1059 1079, doi: [10.1007/s10555-014-9532-2](https://doi.org/10.1007/s10555-014-9532-2).
- [4] P.H. Weigel, B.A. Baggenstoss, What is special about 200 kDa hyaluronan that activates hyaluronan receptor signaling? *Glycobiology* 27 (2017) 868 877, doi: [10.1093/glycob/cwx039](https://doi.org/10.1093/glycob/cwx039).
- [5] S. Patel, P.R. Turner, C. Stubberfield, E. Barry, C.R. Rohlf, A. Stamps, E. McKenzie, K. Young, K. Tyson, J. Terrett, G. Box, S. Eccles, M.J. Page, Hyaluronidase gene profiling and role of hyal-1 overexpression in an orthotopic model of prostate cancer, *Int. J. Cancer.* 97 (2002) 416 424.
- [6] H. Harada, M. Takahashi, CD44-dependent intracellular and extracellular catabolism of hyaluronic acid by hyaluronidase-1 and -2, *J. Biol. Chem.* 282 (2007) 5597 5607, doi: [10.1074/jbc.M608358200](https://doi.org/10.1074/jbc.M608358200).
- [7] H. Yoshida, A. Nagaoka, A. Kusaka-Kikushima, M. Tobiishi, K. Kawabata, T. Sayo, S. Sakai, Y. Sugiyama, H. Enomoto, Y. Okada, S. Inoue, KIAA1199, a deafness gene of unknown function, is a new hyaluronan binding protein involved in hyaluronan depolymerization, *Proc. Natl. Acad. Sci. U. S. A.* 110 (2013) 5612 5617, doi: [10.1073/pnas.1215432110](https://doi.org/10.1073/pnas.1215432110).
- [8] H. Yoshida, A. Nagaoka, S. Nakamura, Y. Sugiyama, Y. Okada, S. Inoue, Murine homologue of the human KIAA1199 is implicated in hyaluronan binding and depolymerization, *FEBS Open Bio* 3 (2013) 352 356, doi: [10.1016/j.fob.2013.08.003](https://doi.org/10.1016/j.fob.2013.08.003).
- [9] H. Yoshida, A. Nagaoka, S. Nakamura, M. Tobiishi, Y. Sugiyama, S. Inoue, N-Terminal signal sequence is required for cellular trafficking and hyaluronan-depolymerization of KIAA1199, *FEBS Lett.* 588 (2014) 111 116, doi: [10.1016/j.febslet.2013.11.017](https://doi.org/10.1016/j.febslet.2013.11.017).
- [10] E.S.A. Hofinger, G. Bernhardt, A. Buschauer, Kinetics of Hyal-1 and PH-20 hyaluronidases: comparison of minimal substrates and analysis of the transglycosylation reaction, *Glycobiology* 17 (2007) 963 971, doi: [10.1093/glycob/cwm070](https://doi.org/10.1093/glycob/cwm070).
- [11] A. Nagaoka, H. Yoshida, S. Nakamura, T. Morikawa, K. Kawabata, M. Kobayashi, S. Sakai, Y. Takahashi, Y. Okada, S. Inoue, Regulation of Hyaluronan (HA) metabolism mediated by HYBID (Hyaluronan-binding protein involved in HA depolymerization, KIAA1199) and HA synthases in growth factor-stimulated fibroblasts, *J. Biol. Chem.* 290 (2015) 30910 30923, doi: [10.1074/jbc.M115.673566](https://doi.org/10.1074/jbc.M115.673566).
- [12] A. Soroosh, S. Albeiroti, G.A. West, B. Willard, C. Fiocchi, C.A. de la Motte, Crohn's disease fibroblasts overproduce the novel protein KIAA1199 to create proinflammatory hyaluronan fragments, *Cell. Mol. Gastroenterol. Hepatol.* 2 (2016) 358 368 e4, doi: [10.1016/j.jcmgh.2015.12.007](https://doi.org/10.1016/j.jcmgh.2015.12.007).
- [13] H. Yoshida, M. Aoki, A. Komiya, Y. Endo, K. Kawabata, T. Nakamura, S. Sakai, T. Sayo, Y. Okada, Y. Takahashi, HYBID (alias KIAA1199/CEMIP) and hyaluronan synthase coordinately regulate hyaluronan metabolism in histamine-stimulated skin fibroblasts, *J. Biol. Chem.* 295 (2020) 2483 2494, doi: [10.1074/jbc.RA119.010457](https://doi.org/10.1074/jbc.RA119.010457).
- [14] H. Yoshida, A. Nagaoka, A. Komiya, M. Aoki, S. Nakamura, T. Morikawa, R. Ohtsuki, T. Sayo, Y. Okada, Y. Takahashi, Reduction of hyaluronan and increased expression of HYBID (alias CEMIP and KIAA1199) correlate with clinical symptoms in photoaged skin, *Br. J. Dermatol.* 179 (2018) 136 144, doi: [10.1111/bjd.16335](https://doi.org/10.1111/bjd.16335).
- [15] H. Yoshida, A. Komiya, R. Ohtsuki, A. Kusaka-Kikushima, S. Sakai, K. Kawabata, M. Kobayashi, S. Nakamura, A. Nagaoka, T. Sayo, Y. Okada, Y. Takahashi, Relationship of hyaluronan and HYBID (KIAA1199) expression with roughness parameters of photoaged skin in Caucasian women, *Skin Res. Technol.* 24 (2018) 562 569, doi: [10.1111/srt.12467](https://doi.org/10.1111/srt.12467).
- [16] C. Deroyer, E. Charlier, S. Neuville, O. Malaise, P. Gillet, W. Kurth, A. Chariot, M. Malaise, D. de Seny, CEMIP (KIAA1199) induces a fibrosis-like process in osteoarthritic chondrocytes, *Cell Death. Dis.* 10 (2019), doi: [10.1038/s41419-019-1377-8](https://doi.org/10.1038/s41419-019-1377-8).
- [17] M. Shimoda, H. Yoshida, S. Mizuno, T. Hirozane, K. Horiuchi, Y. Yoshino, H. Hara, Y. Kanai, S. Inoue, M. Ishijima, Y. Okada, Hyaluronan-binding protein involved in hyaluronan depolymerization controls endochondral ossification through hyaluronan metabolism, *Am. J. Pathol.* 187 (2017) 1162 1176, doi: [10.1016/j.ajpath.2017.01.005](https://doi.org/10.1016/j.ajpath.2017.01.005).
- [18] H. Shimizu, M. Shimoda, S. Mochizuki, Y. Miyamae, H. Abe, M. Chijiwa, H. Yoshida, J. Shiozawa, M. Ishijima, K. Kaneko, A. Kanaji, M. Nakamura, Y. Toyama, Y. Okada, Hyaluronan-binding protein involved in hyaluronan depolymerization is up-regulated and involved in hyaluronan degradation in human osteoarthritic cartilage, *Am. J. Pathol.* 188 (2018) 2109 2119, doi: [10.1016/j.ajpath.2018.05.012](https://doi.org/10.1016/j.ajpath.2018.05.012).
- [19] J. Shiozawa, S. de Vega, M.Z. Cilek, C. Yoshinaga, T. Nakamura, S. Kasamatsu, H. Yoshida, H. Kaneko, M. Ishijima, K. Kaneko, Y. Okada, Implication of HYBID (Hyaluronan-binding protein involved in hyaluronan depolymerization) in hyaluronan degradation by synovial fibroblasts in patients with knee osteoarthritis, *Am. J. Pathol.* (2020), doi: [10.1016/j.ajpath.2020.01.003](https://doi.org/10.1016/j.ajpath.2020.01.003).
- [20] A. Koga, N. Sato, S. Kohi, K. Yabuki, X.-B. Cheng, M. Hisaoka, K. Hirata, KIAA1199/CEMIP/HYBID overexpression predicts poor prognosis in pancreatic ductal adenocarcinoma, *Pancreatol.* (2017) 115-122. [10.1016/j.pan.2016.12.007](https://doi.org/10.1016/j.pan.2016.12.007).
- [21] S. Jia, T. Qu, X. Wang, M. Feng, Y. Yang, X. Feng, R. Ma, W. Li, Y. Hu, Y. Feng, K. Ji, Z. Li, W. Jiang, J. Ji, KIAA1199 promotes migration and invasion by Wnt/ β -catenin pathway and MMPs mediated EMT progression and serves as a poor prognosis marker in gastric cancer, *PLoS One* 12 (2017) e0175058, doi: [10.1371/journal.pone.0175058](https://doi.org/10.1371/journal.pone.0175058).
- [22] N.A. Evensen, C. Kuscu, H.-L. Nguyen, K. Zarrabi, A. Dufour, P. Kadam, Y.-J. Hu, A. Pulkoski-Gross, W.F. Bahou, S. Zucker, J. Cao, Unraveling the role of KIAA1199, a novel endoplasmic reticulum protein, in cancer cell migration, *J. Natl. Cancer Inst.* 105 (2013) 1402 1416, doi: [10.1093/jnci/djt224](https://doi.org/10.1093/jnci/djt224).
- [23] L. Li, L.-H. Yan, S. Manoj, Y. Li, L. Lu, Central role of CEMIP in tumorigenesis and its potential as therapeutic target, *J. Cancer.* 8 (2017) 2238 2246, doi: [10.7150/jca.19295](https://doi.org/10.7150/jca.19295).
- [24] K. Birkenkamp-Demtroder, A. Maghnoji, F. Mansilla, K. Thorsen, C.L. Andersen, B. Øster, S. Hahn, T.F. Ørntoft, Repression of KIAA1199 attenuates Wnt-signalling and

- decreases the proliferation of colon cancer cells, *Br. J. Cancer*. 105 (2011) 552–561, doi: [10.1038/bjc.2011.268](https://doi.org/10.1038/bjc.2011.268).
- [25] D. Zhang, L. Zhao, Q. Shen, Q. Lv, M. Jin, H. Ma, X. Nie, X. Zheng, S. Huang, P. Zhou, G. Wu, T. Zhang, Down-regulation of KIAA1199/CEMIP by miR-216a suppresses tumor invasion and metastasis in colorectal cancer, *Int. J. Cancer*. 140 (2017) 2298–2309, doi: [10.1002/ijc.30656](https://doi.org/10.1002/ijc.30656).
- [26] G. Rodrigues, A. Hoshino, C.M. Kenific, I.R. Matei, L. Steiner, D. Freitas, H.S. Kim, P.R. Oxley, I. Scandariato, I. Casanova-Salas, J. Dai, C.R. Badwe, B. Gril, M. Tešić Mark, B.D. Dill, H. Molina, H. Zhang, A. Benito-Martin, L. Bojmar, Y. Ararso, K. Offer, Q. LaPlant, W. Buehring, H. Wang, X. Jiang, T.M. Lu, Y. Liu, J.K. Sabari, S.J. Shin, N. Narula, P.S. Ginter, V.K. Rajasekhar, J.H. Healey, E. Meylan, B. Costa-Silva, S.E. Wang, S. Rafii, N.K. Altorki, C.M. Rudin, D.R. Jones, P.S. Steeg, H. Peinado, C.M. Ghajar, J. Bromberg, M. de Sousa, D. Pisapia, D. Lyden, Tumour exosomal CEMIP protein promotes cancer cell colonization in brain metastasis, *Nat. Cell Biol.* 21 (2019) 1403–1412, doi: [10.1038/s41556-019-0404-4](https://doi.org/10.1038/s41556-019-0404-4).
- [27] A. Botzki, D.J. Rigden, S. Braun, M. Nukui, S. Salmen, J. Hoehstetter, G. Bernhardt, S. Dove, M.J. Jedrzejas, A. Buschauer, L-Ascorbic acid 6-hexadecanoate, a potent hyaluronidase inhibitor. X-ray structure and molecular modeling of enzyme-inhibitor complexes, *J. Biol. Chem.* 279 (2004) 45990–45997, doi: [10.1074/jbc.M406146200](https://doi.org/10.1074/jbc.M406146200).
- [28] S. Olgen, A. Kaessler, D. Nebioğlu, J. Jose, New potent indole derivatives as hyaluronidase inhibitors, *Chem. Biol. Drug Des.* 70 (2007) 547–551, doi: [10.1111/j.1747-0285.2007.00590.x](https://doi.org/10.1111/j.1747-0285.2007.00590.x).
- [29] L. Udabage, G.R. Brownlee, R. Stern, T.J. Brown, Inhibition of hyaluronan degradation by dextran sulphate facilitates characterisation of hyaluronan synthesis: an in vitro and in vivo study, *Glycoconj. J.* 20 (2004) 461–471, doi: [10.1023/B:GLYC.0000038292.71098.35](https://doi.org/10.1023/B:GLYC.0000038292.71098.35).
- [30] T. Isoyama, D. Thwaites, M.G. Selzer, R.I. Carey, R. Barbucci, V.B. Lokeshwar, Differential selectivity of hyaluronidase inhibitors toward acidic and basic hyaluronidases, *Glycobiology* 16 (2006) 11–21, doi: [10.1093/glycob/cwj036](https://doi.org/10.1093/glycob/cwj036).
- [31] A. Benitez, T.J. Yates, L.E. Lopez, W.H. Cerwinka, A. Bakkar, V.B. Lokeshwar, Targeting hyaluronidase for cancer therapy: antitumor activity of sulfated hyaluronic acid in prostate cancer cells, *Cancer Res.* 71 (2011) 4085–4095, doi: [10.1158/0008-5472.CAN-10-4610](https://doi.org/10.1158/0008-5472.CAN-10-4610).
- [32] A.R. Jordan, S.D. Lokeshwar, L.E. Lopez, M. Hennig, J. Chipollini, T. Yates, M.C. Hupe, A.S. Merseburger, A. Shiedlin, W.H. Cerwinka, K. Liu, V.B. Lokeshwar, Antitumor activity of sulfated hyaluronic acid fragments in pre-clinical models of bladder cancer, *Oncotarget* (2016), doi: [10.18632/oncotarget.10529](https://doi.org/10.18632/oncotarget.10529).
- [33] W. Su, S. Matsumoto, F. Banine, T. Srivastava, J. Dean, S. Foster, P. Pham, B. Hammond, A. Peters, K.S. Girish, K.S. Rangappa, null Basappa, J. Jose, J.D. Hennebold, M.J. Murphy, J. Bennett-Toomey, S.A. Back, L.S. Sherman, A modified flavonoid accelerates oligodendrocyte maturation and functional remyelination, *Glia* 68 (2020) 263–279, doi: [10.1002/glia.23715](https://doi.org/10.1002/glia.23715).
- [34] E. Harunari, C. Imada, Y. Igarashi, T. Fukuda, T. Terahara, T. Kobayashi, Hyaluromycin, a new hyaluronidase inhibitor of polyketide origin from marine *Streptomyces* sp. *Mar. Drugs*. 12 (2014) 491–507, doi: [10.3390/md12010491](https://doi.org/10.3390/md12010491).
- [35] Z. Orlando, I. Lengers, M.F. Melzig, A. Buschauer, A. Hensel, J. Jose, Autodisplay of Human Hyaluronidase Hyal-1 on *Escherichia coli* and Identification of Plant-Derived Enzyme Inhibitors, *Mol. Basel Switz.* 20 (2015) 15449–15468, doi: [10.3390/molecules200915449](https://doi.org/10.3390/molecules200915449).
- [36] G.I. Frost, A.B. Csóka, T. Wong, R. Stern, T.B. Csóka, Purification, cloning, and expression of human plasma hyaluronidase, *Biochem. Biophys. Res. Commun.* 236 (1997) 10–15.
- [37] A.G. Tavianatou, I. Caon, M. Franchi, Z. Piperigkou, D. Galesso, N.K. Karamanos, Hyaluronan: molecular size-dependent signaling and biological functions in inflammation and cancer, *FEBS J.* 286 (2019) 2883–2908, doi: [10.1111/febs.14777](https://doi.org/10.1111/febs.14777).
- [38] I. Kakizaki, H. Koizumi, F. Chen, M. Endo, Inhibitory effect of chondroitin sulfate oligosaccharides on bovine testicular hyaluronidase, *Carbohydr. Polym.* 121 (2015) 362–371, doi: [10.1016/j.carbpol.2014.11.071](https://doi.org/10.1016/j.carbpol.2014.11.071).
- [39] R.H. Jenkins, G.J. Thomas, J.D. Williams, R. Steadman, Myofibroblastic differentiation leads to hyaluronan accumulation through reduced hyaluronan turnover, *J. Biol. Chem.* 279 (2004) 41453–41460, doi: [10.1074/jbc.M401678200](https://doi.org/10.1074/jbc.M401678200).
- [40] A. Boerboom, C. Reusch, A. Pieltain, A. Chariot, R. Franzen, KIAA1199: A novel regulator of MEK/ERK-induced Schwann cell dedifferentiation, *Glia* 65 (2017) 1682–1696, doi: [10.1002/glia.23188](https://doi.org/10.1002/glia.23188).
- [41] H. Morrison, L.S. Sherman, J. Legg, F. Banine, C. Isacke, C.A. Haipek, D.H. Gutmann, H. Ponta, P. Herrlich, The NF2 tumor suppressor gene product, merlin, mediates contact inhibition of growth through interactions with CD44, *Genes Dev.* 15 (2001) 968–980, doi: [10.1101/gad.189601](https://doi.org/10.1101/gad.189601).
- [42] S. Meran, D.W. Thomas, P. Stephens, S. Enoch, J. Martin, R. Steadman, A.O. Phillips, Hyaluronan facilitates transforming growth factor-beta1-mediated fibroblast proliferation, *J. Biol. Chem.* 283 (2008) 6530–6545, doi: [10.1074/jbc.M704819200](https://doi.org/10.1074/jbc.M704819200).
- [43] B. Hinz, Formation and function of the myofibroblast during tissue repair, *J. Invest. Dermatol.* 127 (2007) 526–537, doi: [10.1038/sj.jid.5700613](https://doi.org/10.1038/sj.jid.5700613).
- [44] J. Wang, H. Chen, A. Seth, C.A. McCulloch, Mechanical force regulation of myofibroblast differentiation in cardiac fibroblasts, *Am. J. Physiol. Heart Circ. Physiol.* 285 (2003) H1871–H1881, doi: [10.1152/ajpheart.00387.2003](https://doi.org/10.1152/ajpheart.00387.2003).
- [45] N. Wilson, R. Steadman, I. Muller, M. Draman, D.A. Rees, P. Taylor, C.M. Dayan, M. Ludgate, L. Zhang, Role of Hyaluronan in human adipogenesis: evidence from in-vitro and in-vivo studies, *Int. J. Mol. Sci.* (2019) 20, doi: [10.3390/ijms20112675](https://doi.org/10.3390/ijms20112675).
- [46] L. Bohaumilitzky, A.-K. Huber, E.M. Stork, S. Wengert, F. Woelfl, H. Boehm, A trickster in disguise: Hyaluronan's ambivalent roles in the matrix, *Front. Oncol.* 7 (2017) 242, doi: [10.3389/fonc.2017.00242](https://doi.org/10.3389/fonc.2017.00242).
- [47] A. Seluanov, C. Hine, J. Azpurua, M. Feigenson, M. Bozzella, Z. Mao, K.C. Catania, V. Gorbunova, Hypersensitivity to contact inhibition provides a clue to cancer resistance of naked mole-rat, *Proc. Natl. Acad. Sci. U. S. A.* 106 (2009) 19352–19357, doi: [10.1073/pnas.0905252106](https://doi.org/10.1073/pnas.0905252106).
- [48] X. Tian, J. Azpurua, C. Hine, A. Vaidya, M. Myakishev-Rempel, J. Ablaeva, Z. Mao, E. Nevo, V. Gorbunova, A. Seluanov, High-molecular-mass hyaluronan mediates the cancer resistance of the naked mole rat, *Nature* 499 (2013) 346–349, doi: [10.1038/nature12234](https://doi.org/10.1038/nature12234).
- [49] A. van der Smissen, S. Samsonov, V. Hintze, D. Scharnweber, S. Moeller, M. Schnabelrauch, M.T. Pisabarro, U. Anderegg, Artificial extracellular matrix composed of collagen I and highly sulfated hyaluronan interferes with TGFβ(1) signaling and prevents TGFβ(1)-induced myofibroblast differentiation, *Acta Biomater.* 9 (2013) 7775–7786, doi: [10.1016/j.actbio.2013.04.023](https://doi.org/10.1016/j.actbio.2013.04.023).

- [50] A. van der Smissen, V. Hintze, D. Scharnweber, S. Moeller, M. Schnabelrauch, A. Majok, J.C. Simon, U. Anderegg, Growth promoting substrates for human dermal fibroblasts provided by artificial extracellular matrices composed of collagen I and sulfated glycosaminoglycans, *Biomaterials* 32 (2011) 8938–8946, doi: [10.1016/j.biomaterials.2011.08.025](https://doi.org/10.1016/j.biomaterials.2011.08.025).
- [51] V. Hintze, A. Miron, S. Moeller, M. Schnabelrauch, H.-P. Wiesmann, H. Worch, D. Scharnweber, Sulfated hyaluronan and chondroitin sulfate derivatives interact differently with human transforming growth factor- β 1 (TGF- β 1), *Acta Biomater.* 8 (2012) 2144–2152, doi: [10.1016/j.actbio.2012.03.021](https://doi.org/10.1016/j.actbio.2012.03.021).
- [52] V. Hintze, S. Moeller, M. Schnabelrauch, S. Bierbaum, M. Viola, H. Worch, D. Scharnweber, Modifications of hyaluronan influence the interaction with human bone morphogenetic protein-4 (hBMP-4), *Biomacromolecules* 10 (2009) 3290–3297, doi: [10.1021/bm9008827](https://doi.org/10.1021/bm9008827).
- [53] D.-K. Lim, R.G. Wylie, R. Langer, D.S. Kohane, Selective binding of C-6 OH sulfated hyaluronic acid to the angiogenic isoform of VEGF(165), *Biomaterials* 77 (2016) 130–138, doi: [10.1016/j.biomaterials.2015.10.074](https://doi.org/10.1016/j.biomaterials.2015.10.074).
- [54] V. Hintze, A. Miron, S. Moller, M. Schnabelrauch, S. Heinemann, H. Worch, D. Scharnweber, Artificial extracellular matrices of collagen and sulphated hyaluronan enhance the differentiation of human mesenchymal stem cells in the presence of dexamethasone, *J. Tissue Eng. Regen. Med.* 8 (2014) 314–324, doi: [10.1002/term.1528](https://doi.org/10.1002/term.1528).
- [55] A.C. Midgley, M. Rogers, M.B. Hallett, A. Clayton, T. Bowen, A.O. Phillips, R. Steadman, Transforming Growth Factor- β 1 (TGF- β 1)-stimulated Fibroblast to Myofibroblast Differentiation Is Mediated by Hyaluronan (HA)-facilitated Epidermal Growth Factor Receptor (EGFR) and CD44 Co-localization in Lipid Rafts, *J. Biol. Chem.* 288 (2013) 14824–14838, doi: [10.1074/jbc.M113.451336](https://doi.org/10.1074/jbc.M113.451336).
- [56] S. Hauck, P. Zager, N. Halfter, E. Wandel, M. Torregrossa, A. Kakpenova, S. Rother, M. Ordieres, S. Rathel, A. Berg, S. Moller, M. Schnabelrauch, J.C. Simon, V. Hintze, S. Franz, Collagen/hyaluronan based hydrogels releasing sulfated hyaluronan improve dermal wound healing in diabetic mice via reducing inflammatory macrophage activity, *Bioact. Mater.* 6 (2021) 4342–4359, doi: [10.1016/j.bioactmat.2021.04.026](https://doi.org/10.1016/j.bioactmat.2021.04.026).
- [57] T.Y. Wong, C.-H. Chang, C.-H. Yu, L.L.H. Huang, Hyaluronan keeps mesenchymal stem cells quiescent and maintains the differentiation potential over time, *Aging Cell* 16 (2017) 451–460, doi: [10.1111/ace1.12567](https://doi.org/10.1111/ace1.12567).
- [58] S.K. Nilsson, D.N. Haylock, H.M. Johnston, T. Occhiodoro, T.J. Brown, P.J. Simmons, Hyaluronan is synthesized by primitive hemopoietic cells, participates in their lodgment at the endosteum following transplantation, and is involved in the regulation of their proliferation and differentiation in vitro, *Blood* 101 (2003) 856–862, doi: [10.1182/blood-2002-05-1344](https://doi.org/10.1182/blood-2002-05-1344).
- [59] H.P. Schneider, A. Landsman, *Preclinical and clinical studies of hyaluronic acid in wound care: a case series and literature review*, *wounds compend*, *Clin. Res. Pract.* 31 (2019) 41–48.
- [60] O. De Lucia, A. Murgo, F. Pregnolato, I. Pontikaki, M. De Souza, A. Sinelli, R. Cimaz, R. Caporali, Hyaluronic acid injections in the treatment of osteoarthritis secondary to primary inflammatory rheumatic diseases: a systematic review and qualitative synthesis, *Adv. Ther.* 37 (2020) 1347–1359, doi: [10.1007/s12325-020-01256-7](https://doi.org/10.1007/s12325-020-01256-7).
- [61] W. Zhang, G. Yin, H. Zhao, H. Ling, Z. Xie, C. Xiao, Y. Chen, Y. Lin, T. Jiang, S. Jin, J. Wang, X. Yang, Secreted KIAA1199 promotes the progression of rheumatoid arthritis by mediating hyaluronic acid degradation in an ANXA1-dependent manner, *Cell Death. Dis.* 12 (2021) 1–14, doi: [10.1038/s41419-021-03393-5](https://doi.org/10.1038/s41419-021-03393-5).
- [62] C. Herskind, C. Sticht, A. Sami, F.A. Giordano, F. Wenz, Gene expression profiles reveal extracellular matrix and inflammatory signaling in radiation-induced premature differentiation of Human Fibroblast in vitro, *Front. Cell Dev. Biol.* 9 (2021), doi: [10.3389/fcell.2021.539893](https://doi.org/10.3389/fcell.2021.539893).
- [63] C. Schreiber, S. Saraswati, S. Harkins, A. Gruber, N. Cremers, W. Thiele, M. Rothley, D. Plaumann, C. Korn, O. Armant, H.G. Augustin, J.P. Sleeman, Loss of ASAP1 in mice impairs adipogenic and osteogenic differentiation of mesenchymal progenitor cells through dysregulation of FAK/ Src and AKT signaling, *PLoS Genet.* 15 (2019), doi: [10.1371/journal.pgen.1008216](https://doi.org/10.1371/journal.pgen.1008216).
- [64] A. Schmaus, J.P. Sleeman, Hyaluronidase-1 expression promotes lung metastasis in syngeneic mouse tumor models without affecting accumulation of small hyaluronan oligosaccharides in tumor interstitial fluid, *Glycobiology* 25 (2015) 258–268, doi: [10.1093/glycob/cwu106](https://doi.org/10.1093/glycob/cwu106).
- [65] R. Kunze, M. Rosler, S. Moller, M. Schnabelrauch, T. Riemer, U. Hempel, P. Dieter, Sulfated hyaluronan derivatives reduce the proliferation rate of primary rat calvarial osteoblasts, *Glycoconj. J.* 27 (2010) 151–158, doi: [10.1007/s10719-009-9270-9](https://doi.org/10.1007/s10719-009-9270-9).
- [66] U. Hempel, S. Moller, C. Noack, V. Hintze, D. Scharnweber, M. Schnabelrauch, P. Dieter, Sulfated hyaluronan/collagen I matrices enhance the osteogenic differentiation of human mesenchymal stromal cells in vitro even in the absence of dexamethasone, *Acta Biomater.* 8 (2012) 4064–4072, doi: [10.1016/j.actbio.2012.06.039](https://doi.org/10.1016/j.actbio.2012.06.039).
- [67] M. Schnabelrauch, J. Schiller, S. Moller, D. Scharnweber, V. Hintze, Chemically modified glycosaminoglycan derivatives as building blocks for biomaterial coatings and hydrogels, *Biol. Chem.* (2021), doi: [10.1515/hsz-2021-0171](https://doi.org/10.1515/hsz-2021-0171).
- [68] S. Moller, M. Schmidtke, D. Weiss, J. Schiller, K. Pawlik, P. Wutzler, M. Schnabelrauch, Synthesis and antiherpetic activity of carboxymethylated and sulfated hyaluronan derivatives, *Carbohydr. Polym.* 90 (2012) 608–615, doi: [10.1016/j.carbpol.2012.05.085](https://doi.org/10.1016/j.carbpol.2012.05.085).
- [69] H.G. Lee, M.K. Cowman, An agarose gel electrophoretic method for analysis of hyaluronan molecular weight distribution, *Anal. Biochem.* 219 (1994) 278–287, doi: [10.1006/abio.1994.1267](https://doi.org/10.1006/abio.1994.1267).
- [70] C.A. Schneider, W.S. Rasband, K.W. Eliceiri, NIH Image to ImageJ: 25 years of image analysis, *Nat. Methods.* 9 (2012) 671–675, doi: [10.1038/nmeth.2089](https://doi.org/10.1038/nmeth.2089).
- [71] G. Landini, G. Martinelli, F. Piccinini, Colour deconvolution: stain unmixing in histological imaging, *Bioinforma. Oxf. Engl.* 37 (2021) 1485–1487, doi: [10.1093/bioinformatics/btaa847](https://doi.org/10.1093/bioinformatics/btaa847).
- [72] A.C. Ruifrok, D.A. Johnston, Quantification of histochemical staining by color deconvolution, *Anal. Quant. Cytol. Histol.* 23 (2001) 291–299.
- [73] R.A. Ferrer, A. Saalbach, M. Grunwedel, N. Lohmann, I. Forstreuter, S. Saupe, E. Wandel, J.C. Simon, S. Franz, Dermal fibroblasts promote alternative macrophage activation improving impaired wound healing, *J. Invest. Dermatol.* 137 (2017) 941–950, doi: [10.1016/j.jid.2016.11.035](https://doi.org/10.1016/j.jid.2016.11.035).